2D nonlinear and non-Hertzian gear teeth deflection model for static transmission error calculation

Mechanism and Machine Theory

# 2D Nonlinear and Non-Hertzian Gear Teeth Deflection Model for Static Transmission Error Calculation

--Manuscript Draft--

| | |
|---|---|
| **Manuscript Number:** | MECHMT-D-21-00695R2 |
| **Article Type:** | Research Paper |
| **Keywords:** | spur gears; STE; Nonlinear; non-Hertzian |
| **Corresponding Author:** | Fabio Bruzzone, Ph.D.<br>Politecnico di Torino<br>ITALY |
| **First Author:** | Fabio Bruzzone, Ph.D. |
| **Order of Authors:** | Fabio Bruzzone, Ph.D. |
| | Tommaso Maggi |
| | Claudio Marcellini |
| | Carlo Rosso |
| **Abstract:** | Aim of this paper is to establish a bi-dimensional approach under quasi-static conditions to model the deflection and the load sharing characteristics as well as the contact conditions between engaging teeth in a spur gear transmission. A semi-analytical model is used to obtain tooth deformations and its stiffness, which is employed in an iterative nonlinear scheme to obtain the actual location of the point of application of the load and its intensity between the different teeth pairs. Next a numerical non-Hertzian contact mechanics model is used to obtain surface displacements and pressure distributions accounting for curvature variations and possible tip contacts once equilibrium is established. Several results are shown in terms of static transmission error, load sharing and contact pressures distributions along the roll angle of the gears with and without different kinds and amounts of profile modifications. |
| **Suggested Reviewers:** | Yi Guo<br>yi.guo@nrel.gov |
| | Stephanos Theodossiades<br>S.Theodossiades@lboro.ac.uk |
| | Karsten Stahl<br>stahl@fzg.mw.tum.de |
| **Opposed Reviewers:** | |
| **Response to Reviewers:** | |

POLITECNICO
DI TORINO
Dipartimento di Ingegneria
Meccanica e Aerospaziale

**Prof. Carlo Rosso, Ph.D.**
**Professore di Progettazione meccanica e Costruzione di Macchine (09A3/SSD ING-IND/14)**
***Professor of Machine Design***

**Dear Editor of**
***Mechanism and Machine Theory***

**Torino, April 1st 2021.**

**Object: Submission of original paper**

Dear Editor of Mechanism and Machine Theory,

on behalf of the Authors, I kindly submit the paper "2D Nonlinear and Non-Hertzian gear teeth deflection model for static transmission error calculation", to be considered for publication within Your Journal. We hope that it could be eligible for publication, being an original paper, never submitted nor under submission to other Journals, nor previously published. The paper summarizes the effort of a Ph.D thesis in this field and the constitution of an University Spin Off commercializing the software that implements the proposed methodology.

Actually, the gear dynamic remains a topic of interest because gears are important elements in aerospace, wind turbine and automotive industries.

In particular, we focused our attention on the proper estimation of the static transmission error and its influences on the dynamic answer of the gearbox. In particular, the teeth deflection is the key point for properly compute the exchange of force among the mating teeth and hence the effective displacements of the gears. This paper proposes a methodology for the first step analysis of the influences of micro modifications of the tooth profile on pressure distribution and static transmission error and it compares the results with literature and fully numerical techniques, proving its robustness.

We thank You in advance for Your kind attention, and we remain available to provide every additional information could be useful for publication.

Best regards,

Prof. Carlo Rosso

**Dipartimento di Ingegneria Meccanica e Aerospaziale / Dept. Mechanical and Aerospace Engineering**
Politecnico di Torino Corso Duca degli Abruzzi, 24 – 10129 Torino – Italia
tel: +39 011.090.5817 fax: +39 011.090.6999
carlo.rosso@polito.it www.dimeas.polito.it www.polito.it

Dear Reviewer,

We thank you very much for the effort and time spent to improve our paper and advise us. We have corrected the manuscript with your accurate suggestions. Below are the individual responses to the problems you highlighted.

Reviewer #1: Page 4 line 6:

"with 200.m points" should be written as "with a number of points of 200 times the module m in mm" [for you: 1. we do not use a dot as a multiplier between a numerical factor and a parameter symbol. 2. since a number of points is meant, the units of the module should be stated because otherwise they would be meters according to ISO].

The phrase in question has been updated as you suggested.

Page 5:

Figures 2-a, 2-b, 2-c are still being quoted although Figure 2-a has now been deleted. This paragraph is to be revised.

The quote to the missing portion has been removed and the paragraph revised. Thank you for pointing out this mistake.

Page 10 last word: mean, Page 13 first word: tangent, followed by "mean common tangent". Both should be corrected to "common tangent" without mean.

The phrasing has been corrected.

Page 13:

line 4: cylinder-cylinder and line 6: pinion-gear. Change the hyphens to N-dashes. Line 4 from below: remove the comma.

Hyphens have been changed to N-dashes in both occurrences and the comma has been removed.

Abstract line 9 "tip corner"; page 12 caption of Fig. 6 "tip corner"; page 13 caption of Fig. 7 "tip corner"; page 14 last line "tip corner"; page 15 line 143 "tip corner"; page 16 line 164 "tip corner" and line 166 "corner-tip". What is meant is an edge not a corner (corner is an inside feature), note that in correct gear terminology this is called "tip" only.

Page 28 line 308:

tip-corner contact to be corrected to "tip contact".

The correct terminology as you suggested has been introduced throughout the paper. “Tip contact” is now used everywhere.

Subscripts": The subscripts are upright except if they are RUNNING NUMBERS such as i, j, k, in which case they should be Italics. Please correct in pages 3--13. You can make sure for yourself that this and all the other previous font corrections do comply with ISO 80000.

Subscripts and superscripts have been updated as you suggested. The entire paper now complies with ISO 80000.

Page 28 line 327:

This Glossary is actually a List of Abbreviations, rather.

The title has now been changed into “List of Abbreviations”

References:

[2] second line: gear drives, a bibliography

[13] loaded;  Technical Report no. 3

[20] Beruehrung with capital B;  cannot be Journal, should be "Zeitschrift"

[24] second line: usign to be corrected to using

[28] strength;  strength

[37] second line: formula.,  Remove the fullstop

[43] MMT Vol. 154 is in 2020 not 2021

[44] Non-Hertzian

The problems in the references are now fixed. Thank you again for the insights, we hope that the paper is now suitable for publication.

Kind regards,

The authors.

**Highlights:**

1) A Nonlinear identification of the contact points and load sharing is implemented
2) The proposed methodology overcomes the limitations of Hertzian contact models
3) The proposed model allows precise analyses of 2D gear contact problem
4) The model is validated against different sources and several test cases

# 2D Nonlinear and Non-Hertzian Gear Teeth Deflection Model for Static Transmission Error Calculation

Fabio Bruzzone[a,b,*], Tommaso Maggi[a,b], Claudio Marcellini[a,b], Carlo Rosso[a,b]

[a] *Politecnico di Torino, Corso Duca degli Abruzzi 24, 10100, Torino, Italy*
[b] *GeDy TrAss s.r.l., Via Vincenzo Vela 42, 10128, Torino, Italy*

**Abstract**

Aim of this paper is to establish a bi-dimensional approach under quasi-static conditions to model the deflection and the load sharing characteristics as well as the contact conditions between engaging teeth in a spur gear transmission. A semi-analytical model is used to obtain tooth deformations and its stiffness, which is employed in an iterative nonlinear scheme to obtain the actual location of the point of application of the load and its intensity between the different teeth pairs. Next a numerical non-Hertzian contact mechanics model is used to obtain surface displacements and pressure distributions accounting for curvature variations and possible tip contacts once equilibrium is established. Several results are shown in terms of static transmission error, load sharing and contact pressures distributions along the roll angle of the gears with and without different kinds and amounts of profile modifications.

*Keywords:* Spur gears, STE, Nonlinear, non-Hertzian
*2021 MSC:* 00-01, 99-00

## 1. Introduction

Geared transmissions are commonly used in every field of the industry to transmit, modify and repurpose mechanical shaft power and have been widely studied in literature ([1, 2]), to understand and mitigate the failures they are subjected to. In the early experimental works [3] a dynamic factor was used to compare the nominal conditions to the dynamic ones which were the cause of several types of failures. The sources of excitation of those dynamic conditions are several and very different in nature [4] and are related to the system the gears are operating in, as well as their implicit nature. Torque fluctuations are an obvious source capable of generating vibro-impacts and they are dependent on the inherent characteristics of the power source, for example an internal combustion engine [5], the unsteady aerodynamics in wind turbines [6] or drag torque in vacuum pumps [7] to cite a few examples. Also rotational

*Corresponding author: fabio.bruzzone@polito.it

speed variations, influencing sliding velocity and hence friction can cause gear vibration [8]. Backlash, manufacturing errors as well as the balancing, alignment and positioning of the shafts also play an important role ([9, 10, 11, 12]). However, the main source of excitation comes from the cyclical stiffness variation of the engaging teeth which is an inherent characteristic of gears and can be crystallized in the Static Transmission Error (STE). During the years several methods to compute that stiffness have been proposed, firstly starting from integral approaches ([13, 14]), discrete ones ([15, 16]) or considering the tooth as a trapezoidal beam on top of a rectangular one in a clamped-free condition [17]. Others proposed semi empirical formulas to describe the stiffness considering the rotational speed and the number of actual mating teeth as a function of time and contact ratio ([18, 19]). In all those approaches if contact is considered it is treated as a simple cylinder-to-cylinder contact as described in Hertzian theory [20], thus simplifying several aspects since curvature variations or edges were not considered, while also the location and load applied to the teeth are based on rigid assumptions, not considering the real conditions. With the increase of the availability and computational efficiency many researchers started using Finite Element (FE) to study firstly tooth root stresses or only the structural behavior of the tooth ([21, 22, 23]) neglecting contact entirely or considering it only as a summation of the tooth elastic effect with Hertzian phenomena up to recent years ([24, 25, 26, 27, 28]). The full extent of FE capabilities have been used only as validating tools due to their computational costs, but some hybrid approaches have been proposed, as in [29, 30] in which the FE is used to compute the elastic deflections away from the contact zone, where a detailed contact mechanics model with Semi Analytical (SA) foundations is instead introduced. In this paper a similar approach will be used to compute the STE and the influence of micro-geometrical profile modifications both on the STE and the contact pressures distributions. Indeed, a SA approach well known in literature [16] coupled with further improvements will be used to determine the stiffness of the engagement. However, the location of the contact point and the load sharing characteristics will not be assumed based on the rigid kinematics, but only employed as a starting point for a nonlinear iterative approach searching for the equilibrium of the location of the contact point, the actual number of the engaged teeth pairs and their applied load. Furthermore a detailed non-Hertzian contact mechanics model will be applied to the contacting teeth pairs in equilibrium to precisely estimate the contact pressures even in presence of profile modifications. Indeed this will allow to correctly take into account the continuous curvature variations along the flanks, as well as studying the pressure peaks when edge contact occurs. Firstly the approach to obtain the profile of the tooth is described and the semi-analytical model used to obtain the deflections under load, and hence the stiffness, is shown. Next the nonlinear iterative algorithm is described which aims at obtaining a stable global deformed configuration of the gear pair under load. At this point the non-Hertzian contact model is introduced to describe the deflections and pressure distributions in the contact zone and some results are shown to highlight the importance of a correct modeling of tip contact. Finally several results are shown for a test gear pair

are shown along with a series of comparisons of the effects of different profile modifications on the STE and the load sharing distribution and conclusions are drawn.

## 2. Model description

*Tooth geometry and contact points detection.* In order to have a general and detailed description of the gear teeth surfaces, the profiles are generated by simulating the meshing of a rack cutter tool with a gear blank by implementing the meshing interaction by vector approach as proposed by Litvin [31]. The rack cutter, shown in Figure 1, can be divided in a number of sections depending on the presence or absence of features like semi-topping, which modifies the tip surface, or the protuberance, which acts on the tooth root geometry as well as the root radius of the rack which creates a rounding on the generated tooth. In the reference frame of the cutter the main parameters defining its geometry are namely the module $m$, the pressure angle $\alpha$, the addendum coefficient $h_{\mathrm{a0}}$, the dedendum coefficient $h_{\mathrm{f0}}$, the tip radius coefficient $\rho_{\mathrm{a0}}$. Optionally, depending on the desired tooth geometry also a root radius coefficient $\rho_{\mathrm{f0}}$ can be specified, as well as the semi-topping height and angle ($h_{\mathrm{fp0}}$ and $\alpha_{\mathrm{kp0}}$ respectively) and the protuberance height and angle ($h_{\mathrm{pr,p0}}$ and $\alpha_{\mathrm{pr,p0}}$ respectively). Once the geometry is generated Tooth Profile Modification (TPM) can be further applied, such as tip relief. Other TPM as involute crowning and root relief can be applied using the proposed method, but will not be analyzed in this paper. The location of the contact points will not be defined by the intersections of the profiles with the Line Of Action (LOA) in different angular positions as done in other works ([32, 33, 34, 35]), but will be computed numerically by finding the the pair of nodes, one on the pinion and the other on the driven gear, with the minimal angular distance for each engaged tooth pair. This process will be repeated starting from the rigid conditions with the undeformed geometry as well as in every other iterative step using the deformed profiles as will be detailed later on.

*SA deflections.* The teeth profiles are discretized in $N_{\mathrm{i}}$ points and the bending and shear deformations are computed assuming the tooth as a clamped-free beam with non-uniform geometry using the analytical formula from Cornell [16] instead of the integral approach of Weber [13]. Under a tooth load $F_{\mathrm{j}}$ the expression is

$$\delta_{\mathrm{b}}^{i} = \frac{F_j \cos^2\phi_{\mathrm{l}}'}{E} \sum_{i=1}^{N_i} \delta_i \left[ \frac{l_i^2 - l_{\mathrm{i}}\delta_i + \frac{1}{3}\delta_i^2}{\bar{I}_i} + \frac{2.4(1+\nu) + \tan^2\phi_{\mathrm{l}}'}{\bar{A}_i} \right] \tag{1}$$

where $\delta_i$ is the thickness of the $i^{th}$ slice of the tooth cross-section defined by two consecutive points $i$ and $i+1$ ($i = 1, 2, ..., N_i$) of the profile. $E$ and $\nu$ are respectively the Young's modulus and Poisson coefficient of the material, while $\bar{A}_i$ and $\bar{I}_i$ are the average area and average moment of inertia of the slice, while

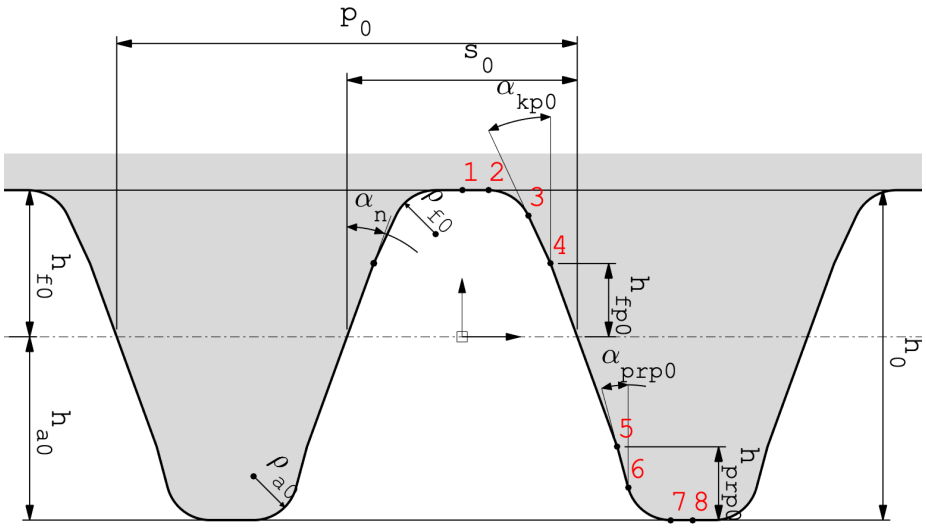


Figure 1: Rack cutter nomenclature.

$\phi'_{\mathrm{l}}$ is the working pressure angle and $l_i$ is the distance of the point of application of the load $F_j$ from the tooth base. The number of points $N_{\mathrm{i}}$ in which the tooth surface is discretized has a very low dependency on the accuracy of the obtained displacements, but a sufficient number is needed for the subsequent contact analysis to correctly represent the contact conditions, therefore in this paper each tooth will be discretized with a number of points 200 times the module $m$ in mm. The contribution to the deformation of the gear body due to the fillet and foundation compliance is based on the theory of elastic rings of Muskhelishvili [36] and its analytical expression is given as [37]

$$\delta_{\mathrm{f}}^{i} = \frac{F_j \cos^2\phi'_{\mathrm{l}}}{bE}\left[L^*\left(\frac{u}{s_{\mathrm{f}}}\right)^2 + M^*\left(\frac{u}{s_{\mathrm{f}}}\right) + P^*\left(1 + Q^*\tan^2\phi'_{\mathrm{l}}\right)\right] \tag{2}$$

where $b$ is the tooth facewidth, $u$ is the height of the intersection between the load and the tooth centerline, while $s_{\mathrm{f}}$ is the chordal thickness of the tooth root base. Coefficients $L^*$, $M^*$, $P^*$, $Q^*$ are estimated by a polynomial function of the form

$$X^*(h_{\mathrm{f},i}, \theta_{\mathrm{f}}) = A_i/\theta_{\mathrm{f}} + B_i h_{\mathrm{f,i}}^2 + C_i h_{\mathrm{f},i}\theta_{\mathrm{f}} + D_i/\theta_{\mathrm{f}} + E_i h_{\mathrm{f},i} + F_i \tag{3}$$

in which the parameters $h_{\mathrm{f},i}$ is the ratio between the root circle radius and the radius of the hub, while $\theta_{\mathrm{f}}$ is half of the tooth angular thickness. The coefficients

Table 1: Polynomial coefficients for Eq. 3

| | $A_i$ | $B_i$ | $C_i$ | $D_i$ | $E_i$ | $F_i$ |
|---|---|---|---|---|---|---|
| $L^*$ | -5.547e-5 | -1.9986e-3 | -2.3015e-4 | 4.7702e-3 | 0.0271 | 6.8045 |
| $M^*$ | 60.111e-5 | 28.100e-3 | -83.431e-4 | -9.9256e-3 | 0.1624 | 0.9086 |
| $P^*$ | -50.952e-5 | 185.50e-3 | 0.05380e-4 | 5.300e-3 | 0.2895 | 0.9236 |
| $Q^*$ | -6.2042e-5 | 9.0889e-3 | -4.0964e-4 | 7.8267e-3 | -0.1472 | 0.6904 |

$A_i$, $B_i$, $C_i$, $D_i$, $E_i$, $F_i$ are given in Table 1. By superposition, the total deflection of a tooth pair $j$ contacting at point $i$ can be defined as

$$\delta_j^i = \left(\delta_{\mathrm{b}}^i\right)_{\mathrm{p}} + \left(\delta_{\mathrm{f}}^i\right)_{\mathrm{p}} + \left(\delta_{\mathrm{b}}^i\right)_{\mathrm{g}} + \left(\delta_{\mathrm{f}}^i\right)_{\mathrm{g}} \tag{4}$$

where the subscript p indicates the deformation of the driving pinion, while g of the driven gear. Those deformations are computed for each point of the profiles and will later be applied to the 2D flanks in the procedure to obtain the equilibrium contact point. Hence, the total stiffness of the engaging teeth pair $j$ contacting in point $i$ can be expressed as

$$k_j^i = \frac{F_j}{\delta_j^i} \tag{5}$$

*Nonlinear algorithm.* It is known that a deformation during contact between two solid bodies can shift the actual contact point from its location predictable by rigid body analysis, especially if bending deformations are involved as is the case for contacting teeth pairs in gears. Indeed, if a rigid body is brought into contact via a vertical displacement with a flexible beam, the first point of contact is easily identifiable by rigid body kinematics. However, if the load is increased, the point of contact will shift, thus changing the deformed shape of the beam. The same reasoning is valid for engaging teeth pairs under load since the contact point identifiable considering the profiles as rigid (Figure 2-a) is indeed different when their deformation under load is taken into account as visible in Figure 2-b and as such cannot be determined a priori. Furthermore in gears the location of the contact point determines the stiffness which in turn determines the fraction of the total load that particular tooth pair will transmit. Numerically, this results in an iterative search in which a natural equilibrium condition is sought for the load, the position of the contact point and the deformed shape of the considered teeth pairs. To start the iterations the load is applied on the rigid contact point of the engaged pairs and the load sharing coefficient for each pair is computed using the ISO 6336 standard [38], thus obtaining the first set of deformed profiles under load. Using this deformed configuration the actual contact points are then obtained. It must be noted that in this step contact is checked between all possible pairs and both anticipated contact or contact loss can happen due to all the effects previously considered. The load sharing coefficient is then updated at the $k^{th}$ iteration using the new

contact point obtained for the $j^{th}$ pair as [39]

$$C_{k,j} = \frac{k_j}{\sum_{i=1}^{N} k_i} \left( \frac{1 + \sum_{i=1}^{N} k_i \tilde{E}_{ji}}{F} \right) \tag{6}$$

where $\tilde{E}_{ji} = \delta_j - \delta_i$ is the STE and $k_j$ is defined in eq. 5 while $F = T/r_\mathrm{b} = \sum_{j=1}^{N} F_j$ where $T$ is the total torque to be transmitted and $r_\mathrm{b}$ is the base radius of the pinion. Equilibrium is reached when the contact points of the different engaging pairs are in a stable position as well as the load sharing coefficients, meaning

$$\frac{x_{k,j} - x_{k-1,j}}{x_{k,j}} < \epsilon_\mathrm{x} \wedge \frac{y_{k,j} - y_{k-1,j}}{y_{k,j}} < \epsilon_\mathrm{y} \wedge \frac{C_{k,j} - C_{k-1,j}}{C_{k,j}} < \epsilon_C \tag{7}$$

where $x_{k,j}$, $y_{k,j}$ are the coordinates of the contact point of the $j^{th}$ engaging pair at the $k^{th}$ iteration and $\epsilon_\mathrm{x}$, $\epsilon_\mathrm{y}$ and $\epsilon_\mathrm{C}$ are tolerance values generally equal to 0.01%. Once equilibrium is reached a detailed contact model, described next, is used to study the contact between the so obtained deformed profiles. A visualization of the described iterative loop applied for every angular position is visible in Figure 3.

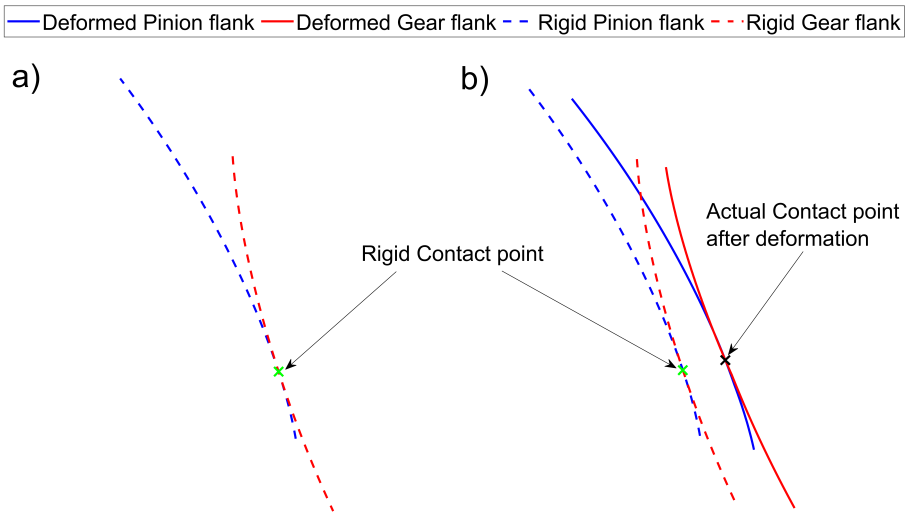


Figure 2: Shift of the actual contact point after deformation, a) rigid contact point of a single tooth pair in engagement, b) actual contact point after deformation.

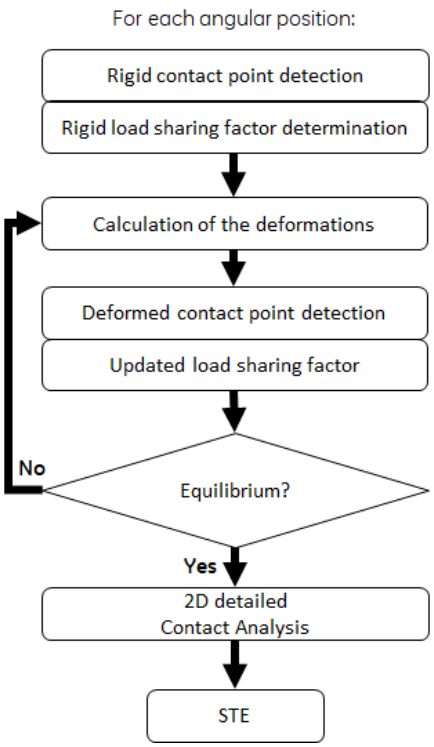


Figure 3: Pseudo-algorithm visualization.

*Non-Hertzian contact model.* Analytical or quasi-analytical contact models [40, 41] as commonly employed in literature in this kind of analytical approaches are not suitable to effectively estimate the contact stiffness and pressures distributions during engagement since they lack the capability to correctly treat the complicated geometry involved. The curvature of the teeth changes continuously due to the intrinsic nature of the involute profile and of the applied tooth deformations, and the above-mentioned models only consider the curvature at the contact point. Furthermore, when tip contact occurs there is no practical way to limit the contact area to where there actually is material to support the pressure, and similar situations occur when tooth profile modifications are to be modeled, such as linear and parabolic tip relief that will be introduced later. When high accuracy is needed the research interest is focused on the FE method [42, 43] with some exceptions [44, 45]. To overcome these limitations and obtain accurate pressure distributions and surface displacements a frictionless non-Hertzian numerical 2D line contact model was implemented. The contact conditions can be expressed in the so called Hertz-Signorini-Moreau problem [46, 47, 48]

$$\mathbf{h} \geq 0, \mathbf{p_n} \geq 0, \mathbf{h} \cdot \mathbf{p_n} = 0, \tag{8}$$

The first condition enforces that no interpenetration can occur between the contact bodies and therefore the gap function $\mathbf{h}$, which measures the distances between the surfaces, can only be positive, or equal to 0 in the contact area. The second condition imposes that the contact is non-adhesive and therefore no tension force must be present in the contact area, formulated from the normal stress

$$\boldsymbol{\sigma_n} = \mathbf{t} \cdot \mathbf{n} \tag{9}$$

where $\mathbf{t}$ is the traction force vector and $\mathbf{n}$ is the normal direction to the surface and $\mathbf{p_n} = -\boldsymbol{\sigma_n}$. The third condition enforces that the normal pressures can only be different from 0 inside the contact area where $\mathbf{h} = 0$ and null everywhere else. The gap function $\mathbf{h}$ is expressed as

$$\mathbf{h} = h_0 + \mathbf{g} + \boldsymbol{\delta} \tag{10}$$

where $h_0$ is the indentation between the profiles imposed as a rigid body motion, $\mathbf{g}$ is the initial separation of the contacting surfaces and represents it topography, while $\boldsymbol{\delta}$ represents the elastic deformation of the surfaces due to the applied normal pressure $\mathbf{p_n}$ and can be expressed as [49]

$$\boldsymbol{\delta} = \mathbf{C} \cdot \mathbf{p_n} \tag{11}$$

where $\mathbf{C}$ is a matrix of the influence coefficients which introduces the elasticity of the contacting surfaces. Its components $C_{ij}(i, j = 0, 1, \ldots N)$ relate the displacement $\delta_i$ at a point $i$ due to the application of a unit pressure at point $j$. If a pressure profile $p_{\mathrm{n}}(x)$ is assumed, the dimensionless elastic deformation

$\delta^*(x)$ can be expressed as [50]

$$\delta^*(x) = -\frac{1}{\pi}\int_{x_\mathrm{a}}^{x_\mathrm{b}} \ln|x_i - x| p_\mathrm{n}(x)\,\mathrm{d}x \tag{12}$$

If the pressure profile is approximated by a piecewise constant function $p_{\mathrm{n},j} = p_\mathrm{n}(x_j)$ in the considered region $x_j - \Delta x/2 \leq x \leq x_j + \Delta x/2$ where $\Delta x$ is the uniform mesh size $\Delta x = x_{j+1} - x_j$, then the deformation at a point $x_i = x_0 + i\Delta x$ can be written as

$$\delta^*(x_i) = -\frac{1}{\pi}\sum_{i=0}^{i=N} C^*_{ij} p_{\mathrm{n},j}\,\mathrm{d}x \tag{13}$$

where

$$C^*_{ij} = \int_{x_j-\Delta x/2}^{x_j+\Delta x/2} \ln|x_i - x|\,\mathrm{d}x \tag{14}$$

which can be solved analytically considering a constant mesh size $\Delta x = x_i - x_j = (i-j)\Delta x$ to yield

$$\begin{aligned} C_{ij} = \frac{4}{E^*}\Bigg[&\left(i-j+\frac{1}{2}\right)\Delta x \cdot \left(\ln\left|\left(i-j+\frac{1}{2}\right)\Delta x\right| - 1\right) \\ &- \left(\left(i-j-\frac{1}{2}\right)\Delta x\right)\cdot\left(\ln\left|\left(i-j-\frac{1}{2}\right)\Delta x\right| - 1\right)\Bigg] \end{aligned} \tag{15}$$

where $E^*$ is the effective elastic modulus considering the material properties of the gears in contact defined as:

$$\frac{1}{E^*} = \left(\frac{1-\nu_1^2}{E_1}\right) + \left(\frac{1-\nu_2^2}{E_2}\right) = \frac{1}{E_1^*} + \frac{1}{E_2^*} \tag{16}$$

Hence, the influence coefficients matrix $\mathbf{C}$ can be decomposed for the contacting bodies as

$$\mathbf{C} = \mathbf{C_1} + \mathbf{C_2} \tag{17}$$

where the influence coefficients of surfaces 1 and 2 are expressed by

$$\begin{aligned} C_{1,ij} = \frac{4}{E_1^*}\Bigg[&\left(i-j+\frac{1}{2}\right)\Delta x \cdot \left(\ln\left|\left(i-j+\frac{1}{2}\right)\Delta x\right| - 1\right) \\ &- \left(\left(i-j-\frac{1}{2}\right)\Delta x\right)\cdot\left(\ln\left|\left(i-j-\frac{1}{2}\right)\Delta x\right| - 1\right)\Bigg] \end{aligned} \tag{18}$$

$$\begin{aligned} C_{2,ij} = \frac{4}{E_2^*}\Bigg[&\left(i-j+\frac{1}{2}\right)\Delta x \cdot \left(\ln\left|\left(i-j+\frac{1}{2}\right)\Delta x\right| - 1\right) \\ &- \left(\left(i-j-\frac{1}{2}\right)\Delta x\right)\cdot\left(\ln\left|\left(i-j-\frac{1}{2}\right)\Delta x\right| - 1\right)\Bigg] \end{aligned} \tag{19}$$

The surfaces displacements can then be obtained from

$$\mathbf{h_s} = \mathbf{C_s p} \tag{20}$$

where $s = 1, 2$. To solve the problem stated in Eq. 8 and satisfy all the conditions a sub-iterative process is needed. Firstly, only the values $h^{\tilde{n}}$ of the nodes $\tilde{n}$ belonging to the domain $x$ that are in actual compenetration and hence satisfy

$$\tilde{n} = \{n \in x \mid h^n < 0\} \tag{21}$$

are selected to form the vector $\tilde{\mathbf{h}}$ and consistently also the corresponding rows and columns of $\mathbf{C}$ are selected to form the matrix $\tilde{\mathbf{C}}$, effectively setting all loads on nodes outside of the contact region to 0. The pressures $\tilde{\mathbf{p}}$ pertaining the compenetrating nodes are obtained by

$$\tilde{\mathbf{p}} = \tilde{\mathbf{C}}^{-\mathbf{1}}\tilde{\mathbf{h}} \tag{22}$$

Next, the list of $\tilde{n}$ nodes is updated by removing those where tensile pressures are registered and those who are not compenetrating anymore due to the elastic deflection of the contacting surfaces, leaving then only those who satisfy

$$\tilde{n} = \{n \in x \mid \mathbf{p} < 0 \wedge \mathbf{Cp} < \mathbf{h}\} \tag{23}$$

This sub-iterative process stops when the list of $\tilde{n}$ nodes at the current sub-iterative step is the same as the previous one. Finally, given a certain $h_0$ after the solution of the sub-iterative procedure just explained, the load acting on the contacting bodies for unit thickness can be found as

$$f = \frac{\Delta x}{2} \sum_{i=0}^{i=N-1} (p_{\mathrm{n},i} + p_{\mathrm{n},i+1}) \tag{24}$$

which in general will be different from the imposed load $F_{\mathrm{j}}$, hence further iterations are needed to obtain the correct $h_0$. A first guess value is used as $h_{0,1}$ for the first iteration, while for the $k^{th}$ iteration the value $h_{0,\mathrm{k}}$ to be used is estimated based on the previous iterations by

$$h_{0,k} = h_{0,k-1} + \frac{h_{0,k-1} - h_{0,k-2}}{f_k - f_{k-1}}(F_j - f_{k-1}) \tag{25}$$

with good convergence rates. The iterations stop when the residual

$$r_k = \frac{F_j - f_k}{F_j} \tag{26}$$

is below a certain tolerance value $\epsilon_{\mathrm{F}}$ so that $r_k \leq \epsilon_{\mathrm{F}}$, where usually $\epsilon_{\mathrm{F}} = 0.01\%$. A visualization of the sub-iterative algorithm to compute the pressure distribution using the proposed approach is visible in Figure 4. Since the equilibrium contact point is known through the algorithm detailed in section

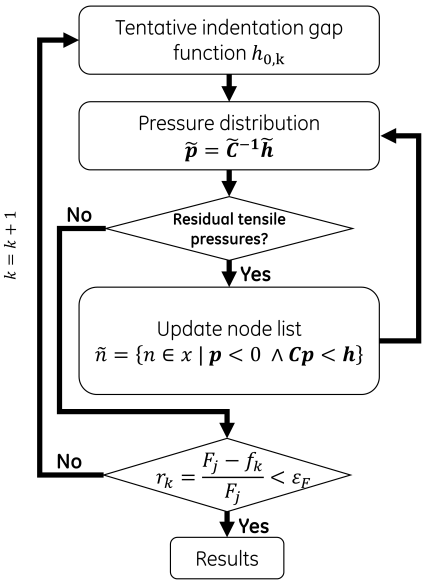


Figure 4: Visualization of the sub-iterative process to compute the pressure distribution using the non-Hertzian model.

Table 2: Gear pair parameters

| Parameter | Pinion | Gear |
|---|---|---|
| Number of teeth $z$ [-] | 28 | 28 |
| Module $m$ [mm] | 3.175 | 3.175 |
| Pressure angle $\alpha_{\mathrm{n}}$ [°] | 20 | 20 |
| Facewidth $b$ [mm] | 6.35 | 6.35 |
| Hub radius [mm] | 20 | 20 |
| Torque $T$ [Nmm] | 101686 | |
| Young modulus $E$ [MPa] | 210000 | 210000 |
| Poisson coefficient $\nu$ [-] | 0.3 | 0.3 |

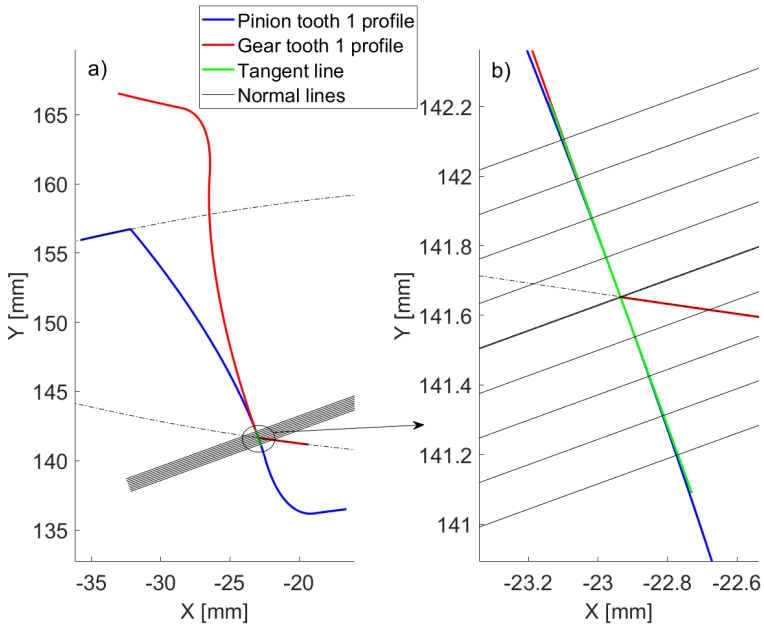


Figure 5: Initial profiles separation **g** estimation a) Full profiles, b) Zoom of the contact region.

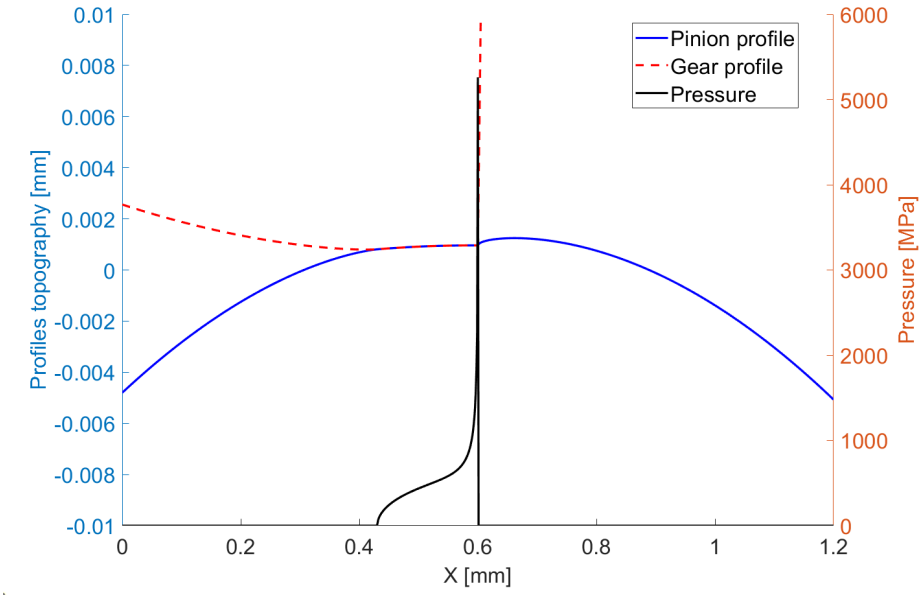


Figure 6: Gear tip contact without modifications.

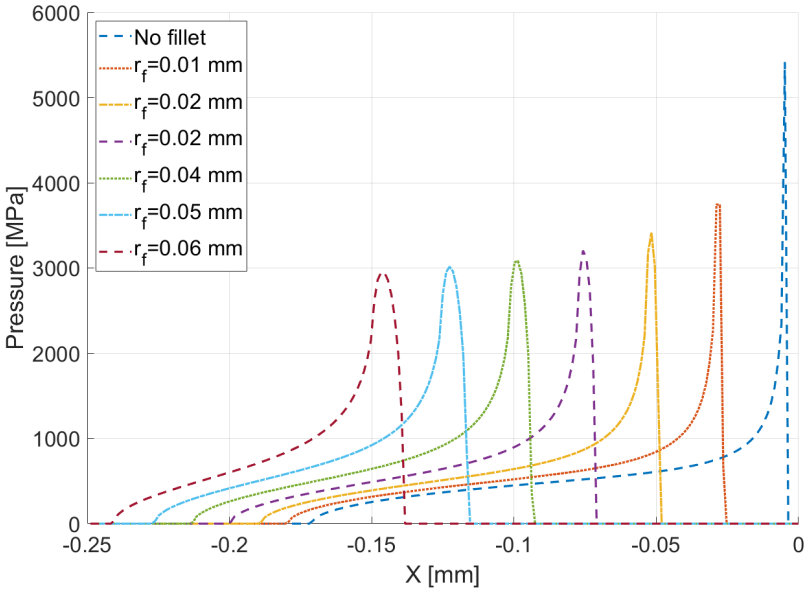


Figure 7: Effect of increasing tip fillet radius on tip contact.

2, the common tangent to both gear profiles is taken as the line where contact will lie. From this line the initial separation $h_0$ as the normal distance between thecommon tangent at the equilibrium contact point and the deformed profiles is obtained. In the cylinder–cylinder contact the imposed rigid body indentation $h_0$ was intended as a vertical displacement of either cylinder towards the other. In the pinion–gear contact instead, in order to respect the meshing kinematics, a rotation is imposed as a rigid body rotation of the pinion towards the gear. Therefore at each iteration it is needed to estimate again the initial separation $\mathbf{g_k}$ obtained through a tentative rigid body rotation $\theta_{0,k}$ for the $k^{th}$ iteration computed in the same way as Eq. 25, hence

$$\theta_{0,k} = \theta_{0,k-1} + \frac{\theta_{0,k-1} - \theta_{0,k-2}}{f_\mathrm{k} - f_{k-1}}(F_j - f_{k-1}) \tag{27}$$

The above method is valid for rough frictionless non-Hertzian contact, but it's still valid also for Hertzian problems, which allows a comparison. Two steel cylinders ($E_1 = E_2 = 210000$ MPa, $\nu_1 = \nu_2 = 0.3$) of radii $r_1 = 100$ mm and $r_2 = 20$ mm are pressed together by a load per unit length varied from 100 N to 1500 N. The maximum pressure values and the estimated contact area from the proposed method, have been compared to Hertz theory [46]. The peak pressure values and the contact area and peak pressure percentage errors are visible in Figure 8 and denote a good accuracy, with an error generally lower than 1%, and a decreasing trend as the load increases since more contact points become

part of the contact area, while in Figure 9 the deformed profiles and the pressure distribution in the contact zone are visibile for a unit length load of 1500 N.

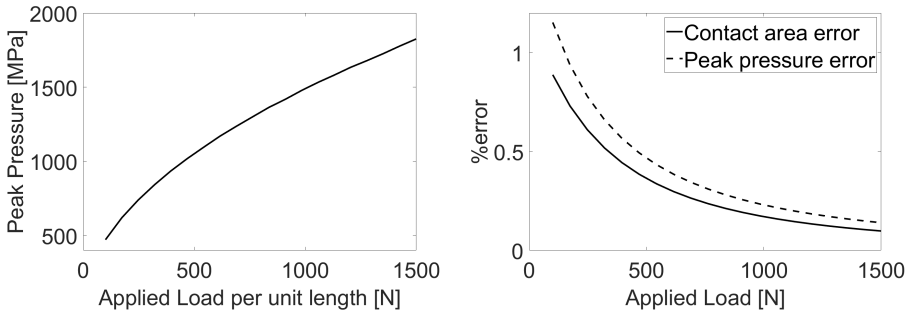


(a) Displacement distribution (b) Contact pressures

Figure 8: Peak pressure variation with increasing load (left), pressure and contact area relative percentage errors (right).

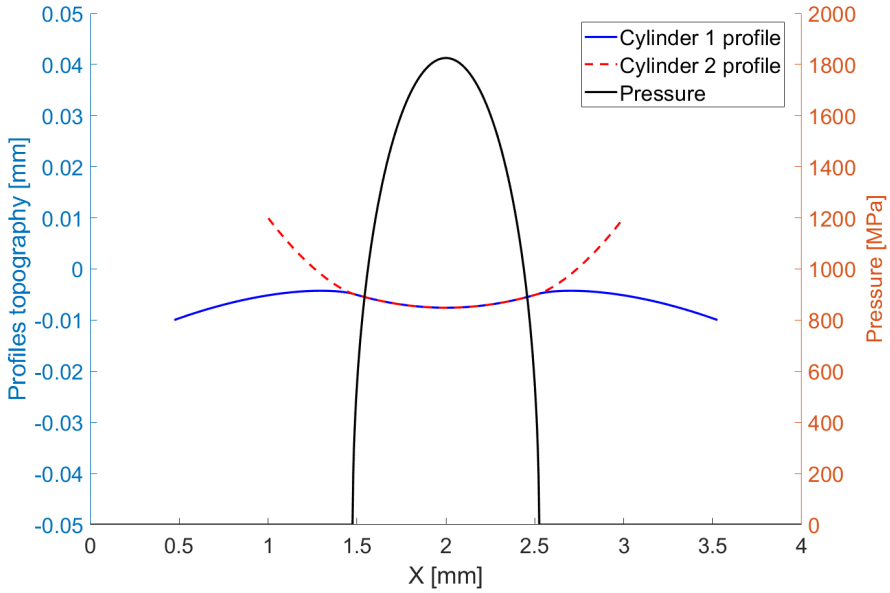


Figure 9: Deformed cylinders profiles and pressure distribution.

*Application to gear contact.* In order to test the proposed method on gear applications where the non-Hertzian approach would show results that a Hertzian approach could not correctly analyze the contact is studied in the angular position when the tip of the gear comes in contact with the flank of the pinion

as in Figure 5. The data of the gear pair considered is listed in Table 2. For a meaningful comparison only one teeth pair will be considered in contact in the position mentioned above and it will hence be applied with the full load $F = T/r_\mathrm{b}$ in order to compare the pressure distribution and highlight the influence of the different profiles modifications. The positioning of the equilibrium contact point and therefore of the contact line results from the iterative algorithm detailed in the previous paragraphs. The deformed profiles and the pressure distribution of an unmodified gear pair are shown in Figure 6 and display an important pressure peak where the sharp tip of the driven gear contacts the flank of the pinion. Although the entity of the pressure peak is exaggerated by the fact that only a single teeth pair is considered taking the full load, this is a better approach than considering the contact as Hertzian. In all upcoming graphs the 0 location of the $x$ axis will be taken as the location of the edge contact point for an unmodified gear in order to also show the different location where contact happens. Indeed, in the industry particular care is taken to avoid this kind of interaction during meshing. Even if no special measure is taken a small tip fillet radius is present due to the machining process of the gears. The magnitude of the fillet tip radius $r_\mathrm{f}$ influences the maximum value of the pressure peak and also the shape of the pressure peak as shown in Figure 7, but this reduction is limited and increasing its value even further would not decrease the overload by much. For this reason, and others as well such as minimizing the fluctuation of the STE and others, more elaborate TPM are usually introduced during manufacturing. The TPM that can be studied in a 2D case are mainly the linear and parabolic tip relief modifications.

*Influence of TPM on pressure distribution.* For the linear tip relief, the modification is characterized by the length of the material to be removed $l_\mathrm{t}$ and by the maximum amount of material to be removed at the outer diameter $\Delta_\mathrm{t}$. As the name implies the amount of material removed decreases linearly from the maximum value $\Delta_\mathrm{t}$ at the tip, to 0 after a length $l_\mathrm{t}$. Similarly, but with a parabolic trend, the parabolic tip relief is characterized by the length of the material to be removed $l_\mathrm{p}$ and by the maximum amount of material to be removed at the outer diameter $\Delta_\mathrm{p}$. Various configurations will now be analyzed to highlight the effects of those modifications on the pressure distribution when tip contact occurs, first for the linear then for the parabolic tip relief. In Figure 10 the length of the material removed $l_\mathrm{t}$ is varied from 0.1 to 0.6 mm with a constant $\Delta_\mathrm{t} = 0.02$ mm. It is evident that increasing the length reduces the maximum pressure experienced by the flank, but usually other considerations have to be taken into account since this increase would retard the approach of the profiles while anticipating the release condition thus increasing the single tooth contact region, which is not always desirable since it reduces the contact ratio. In Figure 11 the $\Delta_\mathrm{t}$ is varied from 0.05 to 0.3 mm with a constant $l_\mathrm{t} = 0.4$ mm. With those values as the material removed increases the maximum pressure increases since a sharp edge is created because a discontinuity in the curvature of the profile is created and this affects the pressure distribution. Regarding the parabolic tip relief in Figure 12 the length of the material

removed $l_p$ is varied from 0.1 to 0.6 mm with a constant $\Delta_p = 0.02$ mm. It is evident that increasing the length reduces the maximum pressure experienced by the flank up to a point where the distribution is almost Hertz-like without any asymmetric pressure peak, but again considerations on the contact ratio must be taken into account. In Figure 13 the $\Delta_p$ is varied from 0.05 to 0.3 mm with a constant $l_p = 0.4$ mm. The parabolic distribution does not cause a discontinuity in the profile of the teeth flank, but however less material is left in the contact zone and therefore a pressure peak becomes progressively more noticeable as the amount of material removed is increased. In the tip contact condition, the non-Hertzian nature of this kind of contact is extremely evident, but when the edge is not involved anymore as the meshing process continues it becomes less important. However, this approach is still more accurate since it considers the real curvature of the involute flank even considering arbitrary modifications and not just the osculating radius at the contact point with constant curvature as in classical analysis. More pressure distribution maps, with the real load distribution among the teeth in contact will be shown in the next section, and the pressure peaks as the teeth come and leave contact will still be evident in the real meshing conditions.

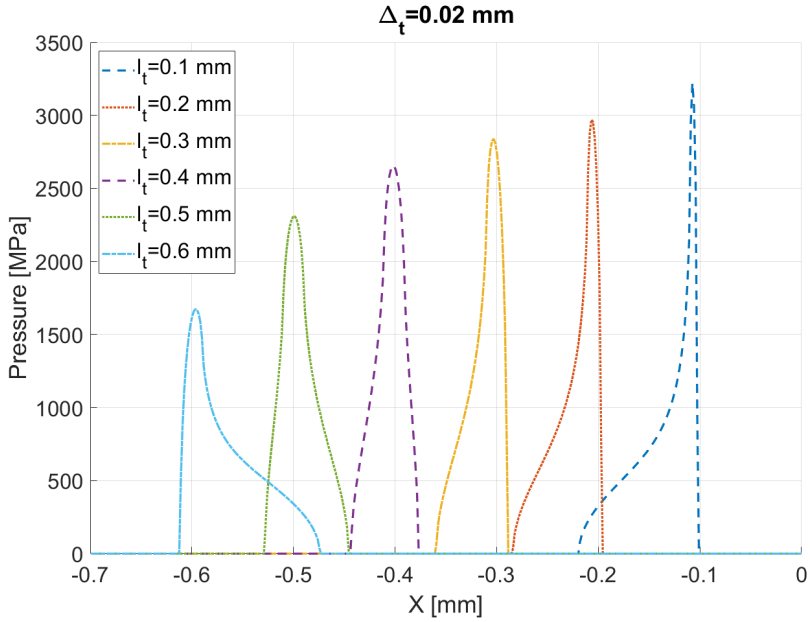


Figure 10: Effect of the increase in length $l_t$ of linear tip relief.

## 3. Application to case studies

In this section the results of the SA approach, considering the superposition of the iterative process and the detailed contact analysis, will be shown. The

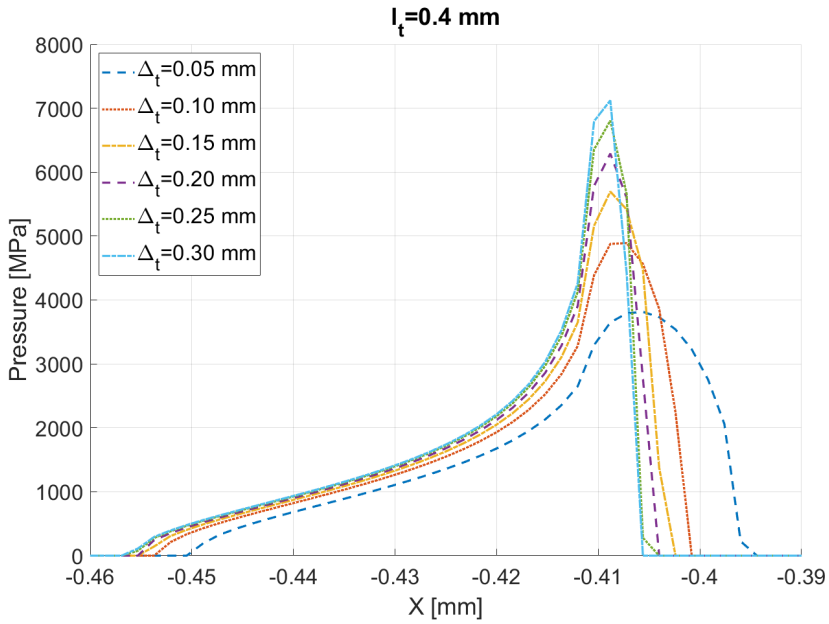


Figure 11: Effect of the increase in depth $\Delta_t$ of linear tip relief.

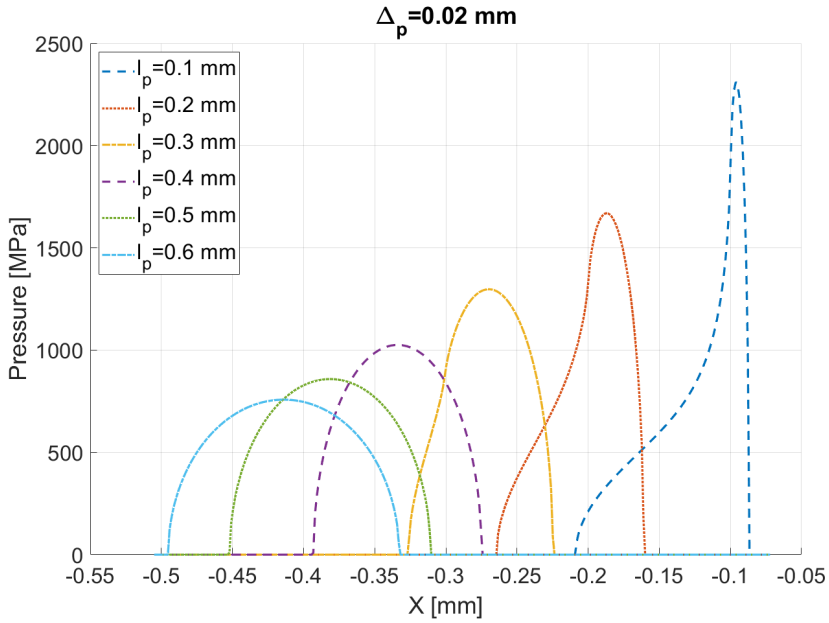


Figure 12: Effect of the increase in length $l_p$ of parabolic tip relief.

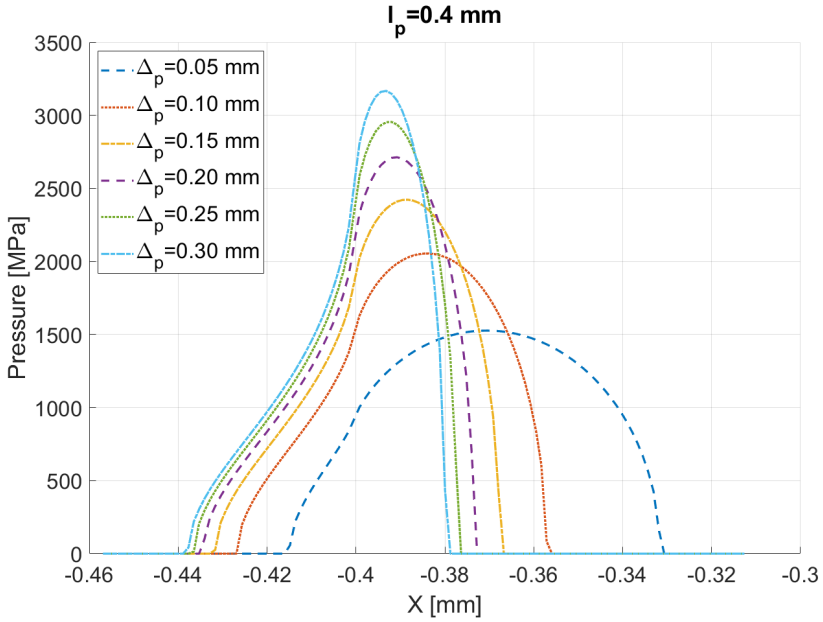


Figure 13: Effect of the increase in depth $\Delta_{\mathrm{p}}$ of parabolic tip relief.

expression for the STE is finally

$$STE = \max\left[\left(\theta_{\mathrm{g}} r_{\mathrm{b,g}} - \theta_{\mathrm{p}} r_{\mathrm{b,p}}\right)_j\right] \tag{28}$$

where the subscript p indicates the pinion rotation, while g indicates the driven gear between the j engaged teeth pairs. The rotations $\theta_{\mathrm{g}}$ and $\theta_{\mathrm{p}}$ are measured at the point of maximum displacement in the contact area from the contact analysis, therefore including also the elastic deflection $\boldsymbol{\delta_{\mathbf{p}}}$ and $\boldsymbol{\delta_{\mathbf{g}}}$. The first comparison of the results from the proposed SA model is against a 2D plane elements FE model from Ansys. In Ansys model only three teeth have been modeled in order to reduce the computational costs since a very refined mesh has been adopted for the contacting flanks of the teeth, which have a mesh size of 0.1 mm to have correct contact results, while the mesh is coarser elsewhere. Quadratic 8-node shell elements (PLANE183) have been used to discretize the geometry, while the deformable contact pair is described by pairs of frictionless contact-target elements (CONTA172-TARGE169) for 2D line contact. The geometrical and material properties are listed in Table 2. The inner diameter of the pinion gear is connected through rigid body connection RBE2 elements to a central node where the torque is applied, and the STE is recorded. The inner diameter of the driven gear is constrained in the same way, but the central node is constrained against all displacements and rotations. An example of the displacements distribution and contact pressures obtained in Ansys is visible in

Figure 14, while the obtained results for one mesh cycle and the comparison against the current method are visible in Figure 15. The agreement between the two is good in terms of overall trend, while at the single contact a difference of $0.3e^{-4}$ rad is present. Ansys results are not symmetric in the mesh cycle due to the lack of adjacent teeth and for the same reason the approach of the following tooth after single contact is slightly retarded with respect to the SA model. The second comparison that has been made has been against the results coming from the Dynamic Analysis of Spur Gear Transmissions (DANST) code from NASA [51]. The tested gears have parameters listed in Table 2 with the exceptions of the data listed in Table 3 and have been analyzed for different levels of torque ranging from 11.3 to 101.7 Nm for one mesh cycle subdivided in 85 intermediate angular positions and the results are visible in Figure 16. Again, the results compare really well except for an upward shift increasing with the torque applied which is constant throughout the meshing process and is probably caused by differences in the formulation employed to model the torsional displacement of the gear body. The two models agree particularly well in the determination of the reduction of the single contact portion of the engagement. In both comparisons no TPM was applied to the gears, but the effect to various levels of torque, ranging from 25.4 Nm to 305.1 Nm, for the same gears tested on the NASA code but this time with a linear tip relief ($\Delta_t = 0.0032$ mm, $l_t = 0.96$ mm) symmetric on both gears are analyzed in Figure 17 over two mesh cycles. As the torque increases also the mean value of the STE increases, but the region of single tooth contact strongly reduces, closely approaching the value of 2 for the highest level of torque. As further comparison the computed gearmesh stiffness obtained from a similar analytical model by Chaari *et al.* [33] is compared to the results from the proposed SA model in Figure 18. Since both models are based on essentially the same formulation the gearmesh stiffness values in single and double contact are extremely close to each other. However small differences can be appreciated since in the proposed SA approach the contact point locations are not based on the geometrical intersections of the profiles with the LOA, thus slightly altering the stiffness values. Furthermore the single contact region is smaller in the proposed approach due to the effect of tooth flexibility under load in the iterative search of the contacting pairs, which is neglected in [33], while also the trend is asymmetric in the mesh cycle since the studied gears have different number of teeth. In the present example the differences are small since the applied torque is low in respect to the stiffness of the studied gear pair, but with higher torque or increased tooth flexibility the differences would be even more evident. In Figure 19 a single STE for the geometry earlier analyzed in the Ansys and DANST comparisons under a torque of 101.7 Nm is visible alongside with the load sharing coefficients for the different engaging teeth pairs.The pressure distribution along the entire mesh process in these conditions is visible Figure 20 and displays the pressure peak as expected and discussed in the previous paragraph. The maximum pressure value is a lot lower than what visible in Figure 6 since in the present case the load acting at the beginning of contact is lower. However, this condition could still cause damage to the flank since the maximum pressure value at the beginning of contact is

Table 3: Gear pair parameters -DANST comparison

| Parameter | Pinion | Gear |
|---|---|---|
| Hub radius [mm] | 10 | 10 |
| Young modulus $E$ [MPa] | 206800 | 206800 |
| Poisson coefficient $\nu$ [-] | 0.29 | 0.29 |

equal to 1414 MPa, which is larger than the maximum value in the single contact zone of the mesh cycle which is 992 MPa, and is usually the value for which gears are designed for. If not accounted for, this pressure peak could cause for example pitting on its surface and must hence be avoided.

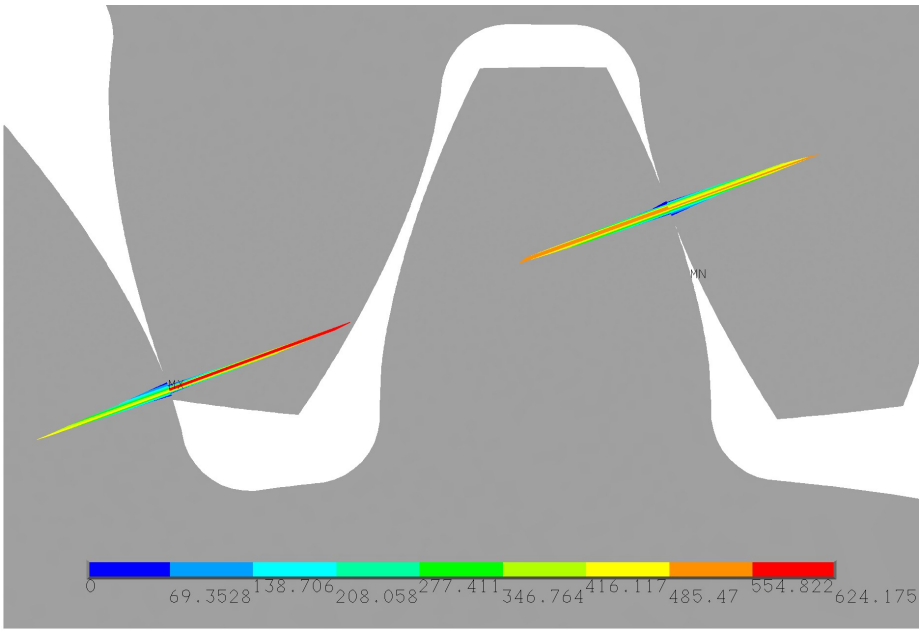


Figure 14: Contact pressures obtained from Ansys at position 0.1/1 in the mesh cycle.

The effect of the linear tip relief is now analyzed. In Figure 21 the effect of the amount of material removed $\Delta_t$ is visible for a fixed length of $l_t = 0.96$ mm. The values are varied from a minimum of 0.01 mm up to 0.04 mm. The main effect is that, as the material removed increases, the length of the single contact zone increases since the teeth pair engage later and leave contact sooner than normal, effectively decreasing the expected contact ratio and leaving the peak to peak value of the STE unchanged. Also, the load sharing coefficient doesn't improve since the passage from double to single contact becomes even more abrupt as the material removed increases, while in the double contact zone the values remain unchanged. In Figure 22 the effect of the length of the linear tip relief is analyzed alongside with the changes it creates in the load

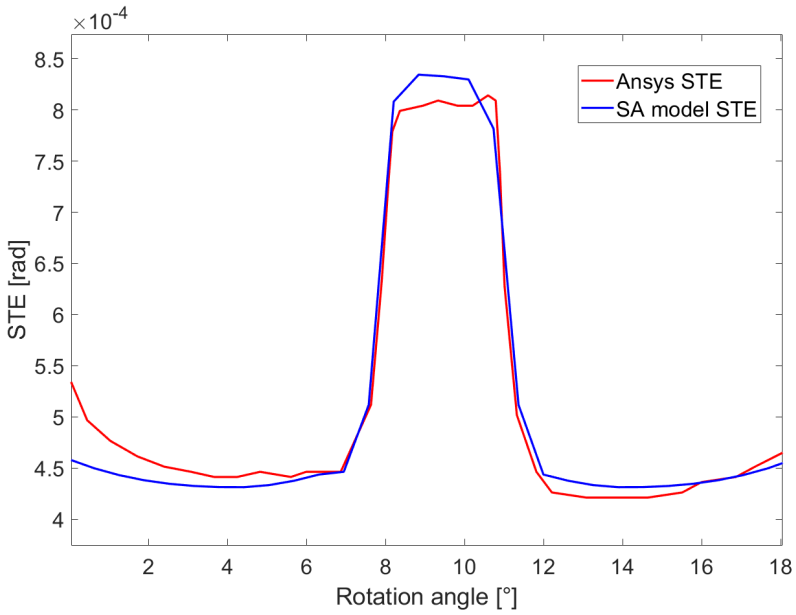


Figure 15: STE results from Ansys and Semi Analytical model.

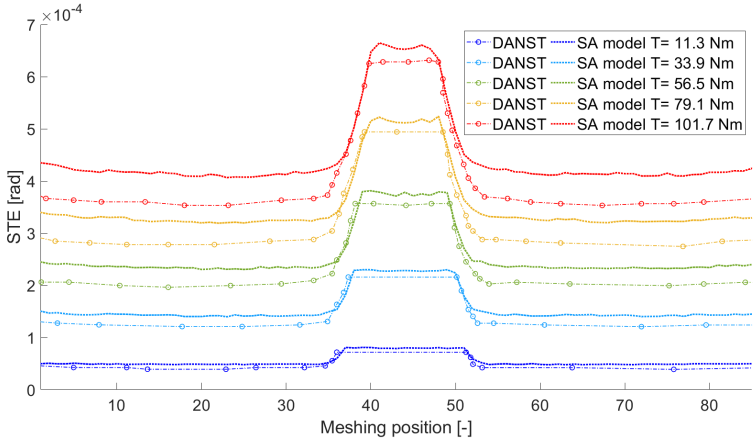


Figure 16: Comparison of NASA DANST results and SA model for several torques.

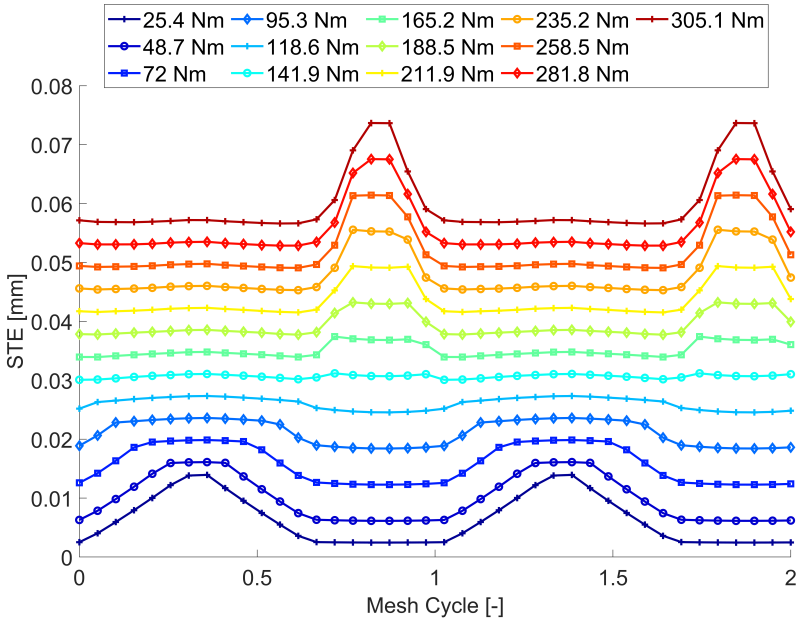


Figure 17: Effect of torque on gears with linear tip relief.

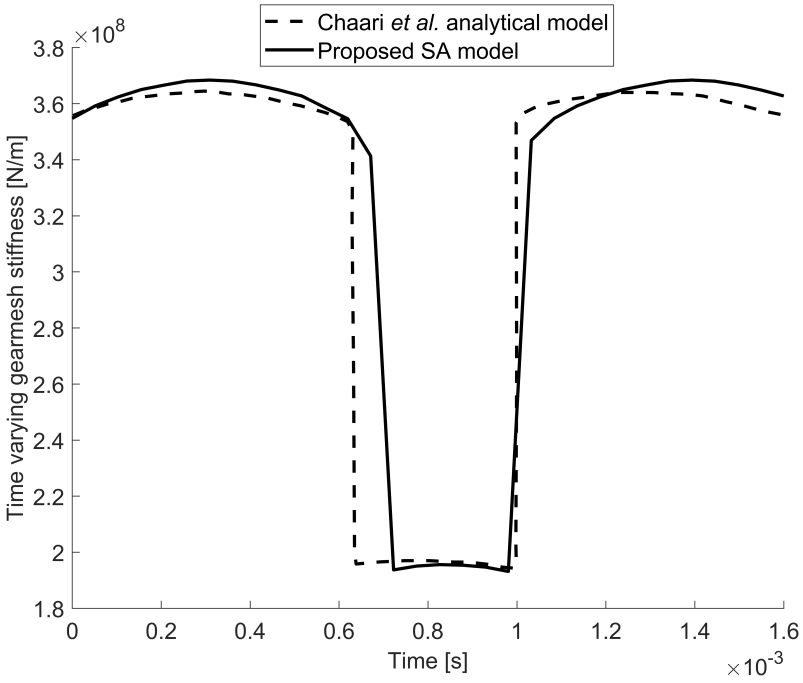


Figure 18: Comparison of gearmesh stiffness from [33] and the proposed SA model.

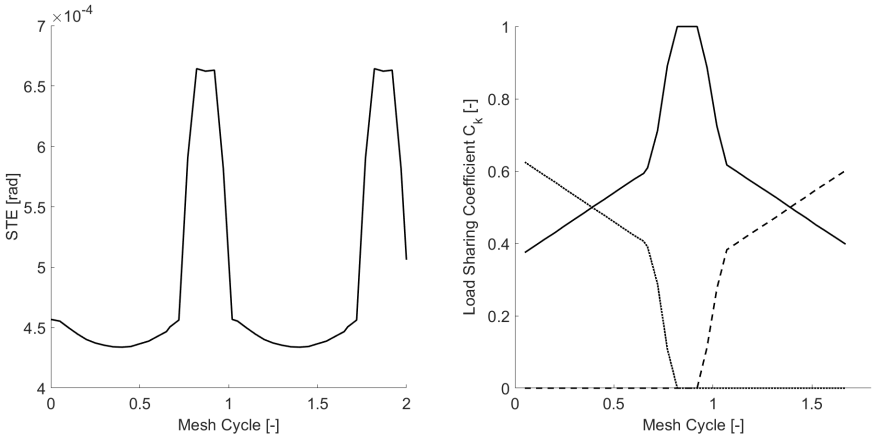


Figure 19: STE and load sharing coefficients without TPM.

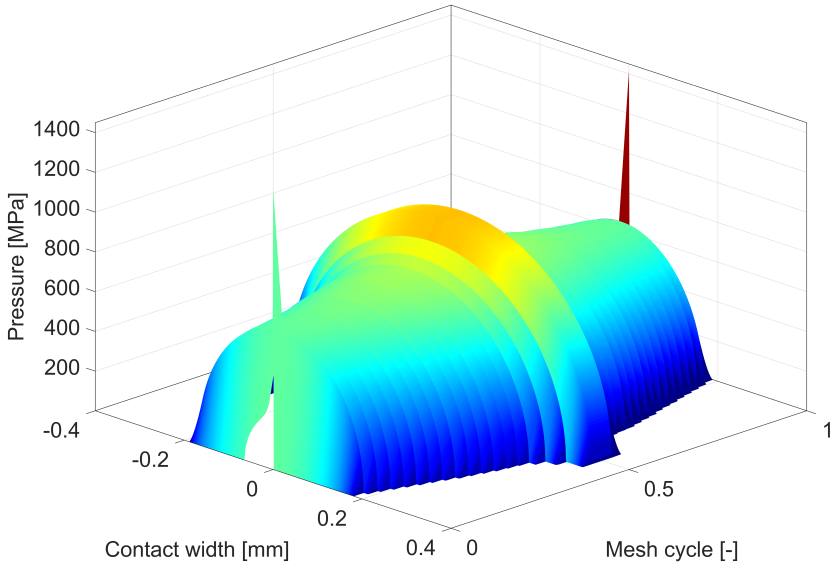


Figure 20: Pressure distribution along the entire mesh process without TPM.

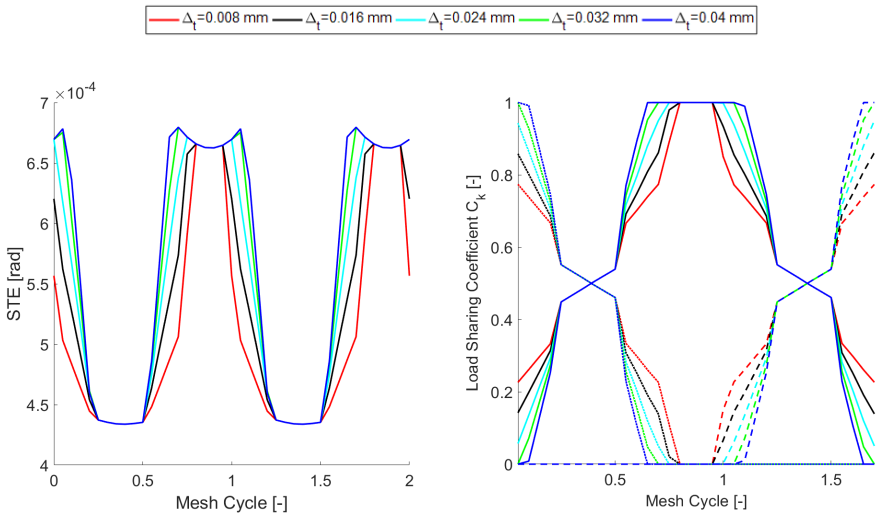


Figure 21: Effect of the variation of the amount of the material removed $\Delta_t$ in linear tip relief TPM $l_t = 0.96$ mm.

sharing coefficients. The length of the material removed $l_t$ is varied from 0.96 mm up to 3 mm and in this case some improvements on both the STE and the load sharing coefficients can be appreciated. Indeed, after a certain value the minimum value of the STE can be seen to increase thus effectively reducing its peak to peak value and at the same time smoothing the transition between the teeth since the fraction of the total load they experience changes without evident discontinuities. In Figure 23 the contact pressure on the flank during the mesh process can be observed for a linear tip relief TPM with $l_t = 0.96$ mm and $\Delta_t = 0.032$ mm and it can be seen that thanks to this modification the pressure peak as the tooth comes into contact is reduced with respect to the unmodified case as in Figure 20. The peak value is equal to 1031 MPa which is still higher than the maximum pressure in the single contact zone of the mesh cycle but is less dangerous than the previous case, since it's only around 40 MPa higher than the design value.

In Figure 24 the effect on the STE and the load sharing coefficients of the amount of material removed in a parabolic tip relief is visible. Its effects are similar to those of the linear tip relief since its only effect is to increase the fraction of the mesh cycle during which single contact occurs. The peak to peak value of the STE remains constant and the load sharing variation doesn't show evident beneficial effects. In Figure 25 the effect of the length of the parabolic tip relief is analyzed and in this case, similarly to what happens for the linear tip relief, some improvements can be seen. As the length of the material removed increase the minimum value of the STE increases and therefore the peak to peak ratio decreases. At the same time, the variation of the load sharing coefficients become smoother as the variation becomes more gradual.

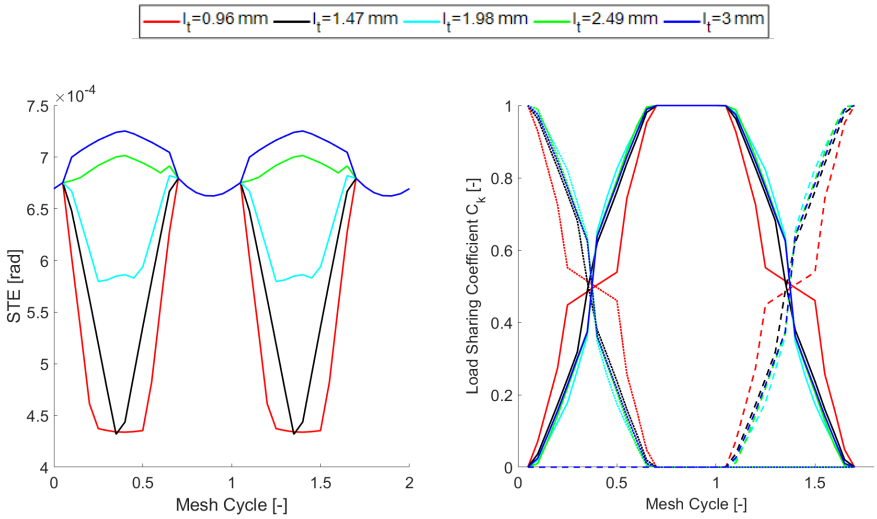


Figure 22: Effect of the variation of the length of the material removed $l_{\mathrm{t}}$ in linear tip relief TPM $\Delta_{\mathrm{t}} = 0.032$ mm.

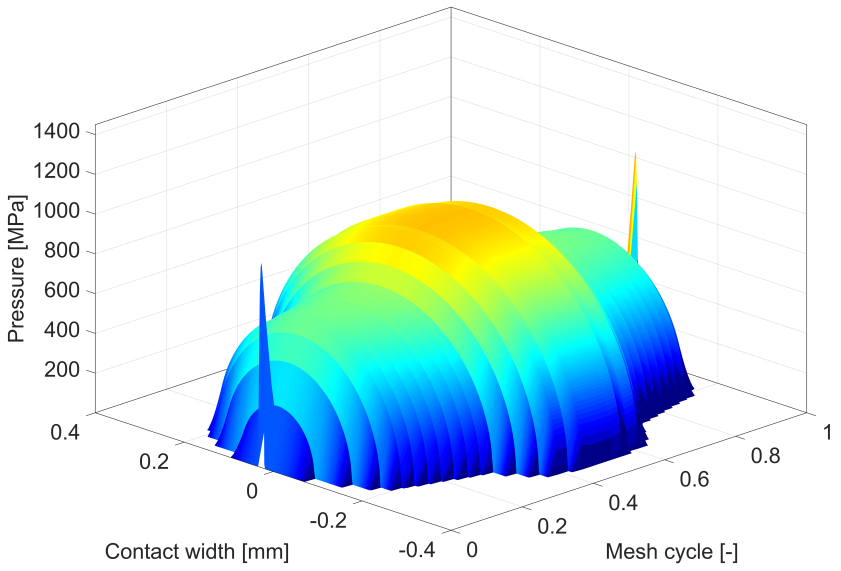


Figure 23: Pressure distribution along the entire mesh process with linear tip relief $l_{\mathrm{t}} = 0.96$ mm and $\Delta_{\mathrm{t}} = 0.032$ mm.

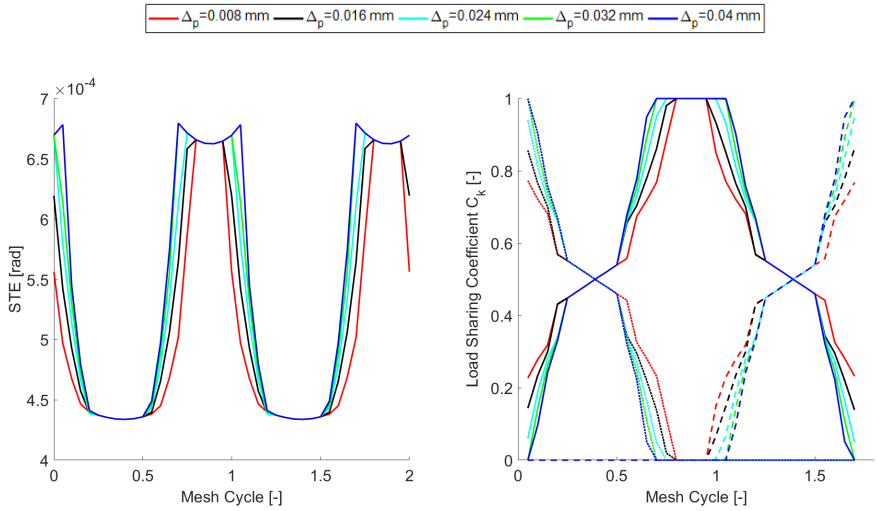


Figure 24: Effect of the variation of the length of the material removed $\Delta_{\mathrm{p}}$ in parabolic tip relief TPM $l_{\mathrm{p}} = 0.96$ mm.

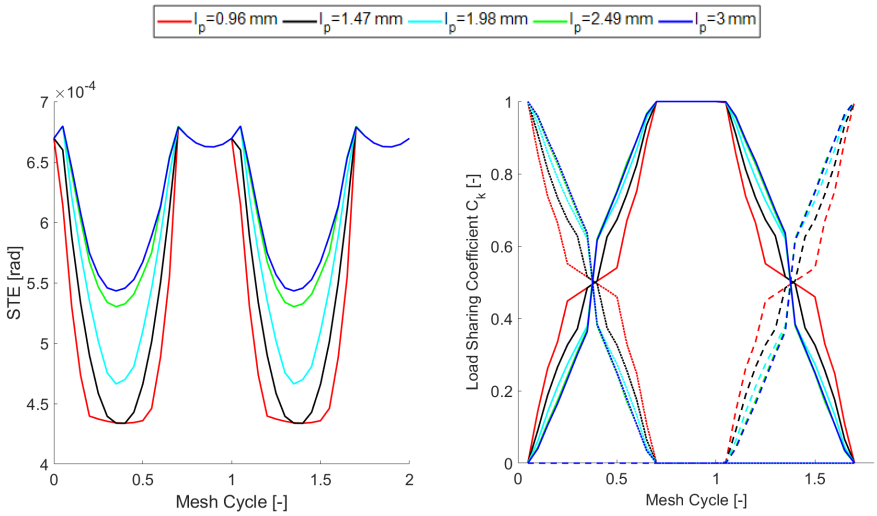


Figure 25: Effect of the variation of the length of the material removed $l_{\mathrm{p}}$ in parabolic tip relief TPM $\Delta_{\mathrm{p}} = 0.032$ mm.

The effect of this modification is lower with respect to the linear tip relief and indeed for the same values of modification the reduction in the peak to peak value of the STE is lower. This is due to the different geometry of the two kind of modifications, since for the same values the volume effectively removed is higher for the linear tip relief, since the amount of material removed increases faster than with respect to the parabolic one. However, the pressure distribution along the entire mesh process for a gear modified with parabolic tip relief with $l_\mathrm{p} = 0.96$ mm and $\Delta_\mathrm{p} = 0.032$ mm can be seen in Figure 26 and this kind of modification is evidently more effective in reducing the pressure peak as the flanks of the gears come into contact. Indeed, the peak is almost completely eliminated (481 MPa) and is just slightly higher than the pressure value when the tip contact effect disappears (430 MPa), but still less than half of the design value in the single tooth contact portion of the mesh cycle and therefore poses no dangers to the integrity of the flank surface.

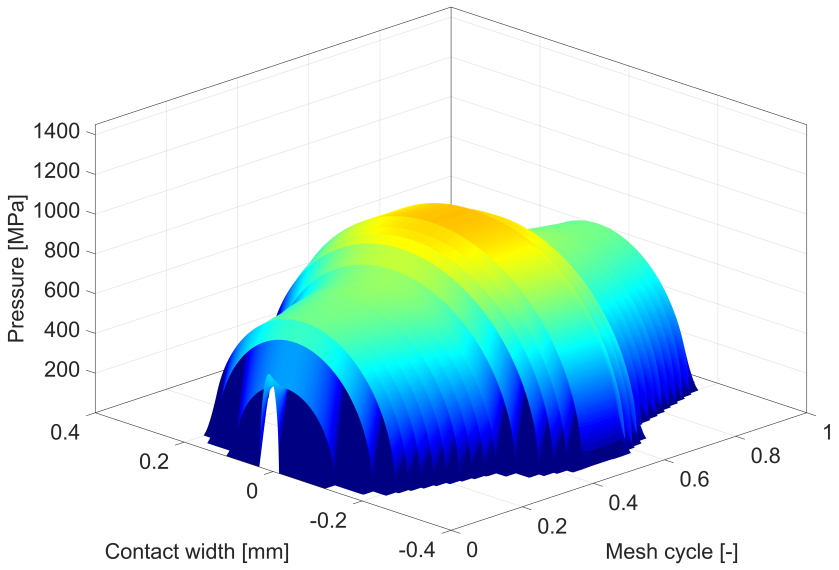


Figure 26: Pressure distribution along the entire mesh process with parabolic tip relief $l_\mathrm{p} = 0.96$ mm and $\Delta_\mathrm{p} = 0.032$ mm.

## 4. Conclusions

Even though gears have been deeply studied and have widespread applications this research field is ever growing. In this paper a novel approach to determine the STE has been detailed. Based on SA foundations well established

in literature regarding the generation of the tooth and the basic stiffness and deformation, this model introduces novel features. A nonlinear iterative approach has been implemented to determine the number of actual engaged tooth pairs, the location of the contact point and the load sharing characteristics without a priori assumptions regarding the position along the line of action or the mesh cycle. This has been achieved aiming for an equilibrium condition of the SA model in terms of deformations and load. Furthermore, whereas in literature the contact between gears is commonly treated with simplified approaches, like considering it as a cylinder-cylinder contact with constant curvature radii, here it has been treated in much more detail. A non-Hertzian contact mechanics model has been applied to the equilibrium deformed profiles to study particular conditions, usually neglected, such as the tip contact that can happen when a teeth pair begins its engagement. Several results have been presented to expose the effects that different TPM can have on this phenomenon. After a validation of the accuracy of the approach against a FE model and results available in literature finally results of the complete approach in terms of STE, load sharing characteristics and contact pressures along the engagement have been shown for different combinations of TPM and their differences and effects have been highlighted. The results given here are just examples of the capabilities of the proposed model, but it is clear that in order to achieve a good gear design those analyses alone are not enough. Indeed, a combinatory analysis taking into account the design loads and the possible combination of the macro (module, pressure angle, profile shift, etc.. . . ) and micro (tip or root relief, kind of TPM, length and amount of material removed) have to be considered at the same time so as to create a response surface in which the effects of all parameters are linked and can therefore be used to estimate the better combination to improve the reliability, wear resistance, fatigue life or noise related issues depending on the objective or objectives of the analysis. This optimization approach, common in literature ([52, 53, 54]), is not in the scope of the current work but will be object of future research.

### List of Abbreviations

**DANST** Dynamic Analysis of Spur Gear Transmissions. 19

**FE** Finite Element. 2

**LOA** Line Of Action. 3

**SA** Semi Analytical. 2

**STE** Static Transmission Error. 2

**TPM** Tooth Profile Modification. 3

## References


[1] B. Abersek, J. Flasker, S. Glodez, Review of mathematical and experimental models for determination of service life of gears, Engineering Fracture Mechanics 71 (2004) 439–453.

[2] L. Prasil, J. Mackerle, Finite element analyses and simulations of gears and gear drives, a bibliography 1997-2006, International Journal for Computer-Aided Engineering and Software 25 (2008) 196–219.

[3] H. N. Ozguven, D. R. Houser, Mathematical models used in gear dynamics - a review, Journal of Sound and Vibration 121 (1988) 383–411.

[4] F. Bruzzone, C. Rosso, Sources of excitation and models for cylindrical gear dynamics: a review, Machines 8 (2020) 37.

[5] Y. Kadmiri, J. Perret-Liaudet, E. Rigaud, A. Le Bot, L. Vary, Influence of multiharmonics excitation on rattle noise in automotive gearboxes, Advances in Acoustics and Vibration 2011 (2011) 659797.

[6] I. Bel Mabrouk, A. El Hami, L. Walha, B. Zghal, Dynamic vibrations in wind energy systems: Application to vertical axis wind turbine, Mechanical Systems and Signal Processing 85 (2017) 396–414.

[7] P. Garambois, G. Donnard, E. Rigaud, J. Perret-Liaudet, Multiphysics coupling between periodic gear mesh excitation and input/output fluctuating torques: Application to a roots vacuum pump, Journal of Sound and Vibration 405 (2017) 158–174.

[8] H. Jiang, F. Liu, Dynamic modeling and analysis of spur gears considering friction–vibration interactions, Journal of Brazilian Society of Mechanical Science and Engineering 39 (2017) 4911–4920.

[9] S. Theodossiades, S. Natsiavas, Non-linear dynamics of gear-pair systems with periodic stiffness and backlash, Journal of Sound and Vibration 229 (2000) 287–310.

[10] J. Hedlund, A. Lehtovaara, Testing method for the evaluation of parametric excitation of cylindrical gears, Nondestructive Testing and Evaluation 23 (2008) 285–299.

[11] N. Inavolu, S. N. Kamani, R. M. Jaganmohan, Driveline noise source identification and reduction in commercial vehicles, SAE Technical Paper 2018-01-1474.

[12] F. Guo, Z. Fang, The statistical analysis of the dynamic performance of a gear system considering random manufacturing errors under different levels of machining precision, Proceedings of the Institution of Mechanical Engineers, Part C: Journal of Mechanical Engineering Science 234 (2020) 3–18.

[13] C. Weber, The deformation of load gears and the effect on their load-carrying capacity. Technical Report no. 3, British Department of Scientific and Industrial Research, London, 1949.

[14] C. Weber, K. Banaschek, Formänderung und Profilrücknahme be gerad- und schraegverzahnten Raedern, Vieweg, Braunschweig, 1953.

[15] R. W. Cornell, W. W. Westervelt, Dynamic tooth loads and stressing for high contact ratio spur gears, Transactions of the American Society of Mechanical Engineers, Journal of Mechanical Design 100 (1978) 69–76.

[16] R. W. Cornell, Compliance and stress sensitivity of spur gear teeth, Journal of Mechanical Design 103 (1981) 447–459.

[17] J. Ishikawa, Fundamental investigations on the design of spur gears, Bull of T.I.T 197 (1957) 55–62.

[18] Y. Cai, T. Hayashi, The optimum modification of tooth profile of power transmission spur gears to make the rotational vibration equal zero, Transactions of the Japan Society of Mechanical Engineers 57 (1991) 3957–3963.

[19] Y. Cai, T. Hayashi, The linear approximated equation of vibration of a pair of spur gears, Journal of Mechanical Design 116 (1994) 558–564.

[20] H. R. Hertz, Über die berührung fester elastischer Körper, Zeitschrift für die reine und angewandte Mathematik 92 (1881) 156–171.

[21] G. Deng, T. Nakanishi, K. Inoue, Bending load capacity enhancement using an asymmetric tooth profile, JSME International Journal Series C 46 (2003) 1171–1177.

[22] T. Lin, H. Ou, R. Li, A finite element method for 3d static and dynamic contact/impact analysis of gear drives, Computer Methods in Applied Mechanics and Engineering 196 (2007) 1716–1728.

[23] N. L. Pedersen, M. F. Jorgenses, On gear tooth stiffness evaluation, Computers and Structures 135 (2014) 109–117.

[24] M. H. Arafa, M. M. Megahed, Evaluation of spur gear mesh compliance using the finite element method, Proceedings of the Institution of Mechanical Engineers, Part C: Journal of Mechanical Engineering Science 213 (1999) 569–579.

[25] W. Hu, Z. Chen, A multi-mesh mpm for simulating the meshing process of spur gears, Computers and Structures 81 (2003) 1991–2002.

[26] J. D. Wang, I. M. Howard, Error analysis of finite element modeling of involute spur gears, Journal of Mechanical Design 128 (2006) 90–97.

[27] S. He, R. Gunda, R. Singh, Effect of sliding friction on the dynamics of spur gear pair with realistic time-varying stiffness, Journal of Sound and Vibration 301 (2007) 927–949.

[28] S. Li, Finite element analyses for contact strength and bending strength of a pair of spur gears with machining errors, assembly errors and tooth modifications, Mechanism and Machine Theory 42 (2007) 88–114.

[29] R. G. Parker, S. M. Vijayakar, T. Imajo, Non-linear dynamic response of a spur gear pair: Modelling and experimental comparisons, Journal of Sound and Vibration 237 (2000) 435–455.

[30] Y. Guo, T. Eritnel, T. M. Ericson, R. G. Parker, Vibro-acoustic propagation of gear dynamics in a gear-bearing-housing system, Journal of Sound and Vibration 333 (2014) 5762–5785.

[31] F. L. Litvin, Gear geometry and applied theory, P. T. R. Prentice Hall, 1994.

[32] A. Fernandez del Rincon, F. Viadero, M. Iglesias, A. de Juan, R. Sancibrian, A model for the study of meshing stiffness in spur gear transmissions, Nondestructive Testing and Evaluation 61 (2013) 30–58.

[33] F. Chaari, T. Fakhfakh, M. Haddar, Analytical modelling of spur gear tooth crack and influence on gearmesh stiffness, European Journal of Mechanics - A/Solids 28 (2009) 461–468.

[34] A. Y. Tesfahuneng, F. Rosa, C. Gorca, The effects of the shape of tooth profile modifications on the transmission error, bending and contact stress of spur gears, Proceedings of the Institution of Mechanical Engineering Part C: Journal of Mechanical Engineering Science 224 (2010) 1749–1758.

[35] V. Nikolic, C. Dolicanin, D. Dimitrijevic, Dynamic model for the stress and strain state analysis of a spur gear transmission, Journal of Mechanical Engineering 58 (2012) 56–67.

[36] N. Muskhelishvili, Some basic problems of the mathematical theory of elasticity, Springer Netherlands, Heidelberg, 1975.

[37] P. Sainsot, P. Velex, O. Duverger, Contribution of gear body to tooth deflections - a new bidimensional analytical formula, Journal of Mechanical Design 126 (2004) 748–752.

[38] ISO 6336-1:2019 Calculation of load capacity of spur and helical gears, Standard, International Organization for Standardization, Geneva, CH (2019).

[39] H. Ma, X. Pang, R. J. Feng, J. Zeng, B. C. Wen, Improved time-varying mesh stiffness model of cracked spur gears, Engineering Failure Analysis 55 (2015) 271–287.

[40] P. Sainsot, P. Velex, On contact deflection and stiffness in spur and helical gears, Mechanism and Machine Theory 154 (2020) 104049.

[41] V. I. Medvedev, A. E. Volkov, M. A. Volosova, O. E. Zubelevich, Mathematical model and algorithm for contact stress analysis of gears with multi-pair contact, Mechanism and Machine Theory 86 (2015) 156–171.

[42] H. X., Z. Fang, X. Zhang, Static contact analysis of spiral bevel gear based on modified VFIFE (vector form intrinsic finite element) method, Applied Mathematical Modelling 60 (2018) 192–207.

[43] A. Beinstingel, M. Keller, M. Heider, B. Pinnekamp, S. Marburg, A hybrid analytical-numerical method based on isogeometric analysis for determination of time varying mesh stiffness, Mechanism and Machine Theory 154 (2020) 104049.

[44] N. Pop, S. Cretu, A. Tufescu, Non-hertzian contact model for tooth contact analysis of spur gear with lead crowning, Applied Mechanics and Materials 658 (2014) 351–356.

[45] Q. Wen, Q. Du, X. Zhai, An analytical method for calculating the tooth surface contact stress of spur gears with tip relief, International Journal of Mechanical Sciences 151 (2019) 170–180.

[46] K. L. Johnson, Contact mechanics, Cambridge University Press, Cambridge, 1985.

[47] J. J. Kalker, Three-dimensional elastic bodies in rolling contact, Springer Netherlands, 1990.

[48] P. Wriggers, Computational contact mechanics, Springer, 2002.

[49] R. S. Sayles, Basic principles of rough surface contact analysis using numerical methods, Tribology International 29 (1996) 639–650.

[50] C. H. Venner, Multilevel solution of the EHL line and point contact problems, Ph.D Thesis, University of Twente, Twente, 1963.

[51] F. B. Oswald, H. H. Lin, R. Delgado I., Dynamic analysis of spur gear transmissions (DANST). pc version 3.00 user manual, NASA Technical Report 107291 (1996) 1–26.

[52] N. Amini, B. G. Rosen, H. Westberg, Optimization of gear tooth surfaces, International Journal of Machine Tools and Manufacture 38 (1998) 425–435.

[53] A. L. Kapelevich, Y. V. Shekhtman, Direct gear design: Bending stress minimization, Gear Technology 20 (2003) 44–47.

[54] Y. M. Mohan, T. Seshaiah, Spur gear optimization by using genetic algorithm, International Journal of Engineering Research and Applications 2 (2012) 331–318.

Click here to access/download

**LaTeX Source File**

MaMT_template.rar

Conflict of Interest and Authorship Conformation Form

Please check the following as appropriate:

- ✓ All authors have participated in (a) conception and design, or analysis and interpretation of the data; (b) drafting the article or revising it critically for important intellectual content; and (c) approval of the final version.
- ✓ This manuscript has not been submitted to, nor is under review at, another journal or other publishing venue.
- o The authors have no affiliation with any organization with a direct or indirect financial interest in the subject matter discussed in the manuscript
- ✓ The following authors have affiliations with organizations with direct or indirect financial interest in the subject matter discussed in the manuscript:

| Author's name | Affiliation |
|---|---|
| Fabio Bruzzone | Politecnico di Torino – GeDy TrAss s.r.l. |
| Tommaso Maggi | Politecnico di Torino – GeDy TrAss s.r.l. |
| Claudio Marcellini | Politecnico di Torino – GeDy TrAss s.r.l. |
| Carlo Rosso | Politecnico di Torino – GeDy TrAss s.r.l. |
| | |
| | |
| | |
| | |

# 2D Nonlinear and Non-Hertzian Gear Teeth Deflection Model for Static Transmission Error Calculation

Fabio Bruzzone[a,b,*], Tommaso Maggi[a,b], Claudio Marcellini[a,b], Carlo Rosso[a,b]

[a] *Politecnico di Torino, Corso Duca degli Abruzzi 24, 10100, Torino, Italy*
[b] *GeDy TrAss s.r.l., Via Vincenzo Vela 42, 10128, Torino, Italy*

**Abstract**

Aim of this paper is to establish a bi-dimensional approach under quasi-static conditions to model the deflection and the load sharing characteristics as well as the contact conditions between engaging teeth in a spur gear transmission. A semi-analytical model is used to obtain tooth deformations and its stiffness, which is employed in an iterative nonlinear scheme to obtain the actual location of the point of application of the load and its intensity between the different teeth pairs. Next a numerical non-Hertzian contact mechanics model is used to obtain surface displacements and pressure distributions accounting for curvature variations and possible tip contacts once equilibrium is established. Several results are shown in terms of static transmission error, load sharing and contact pressures distributions along the roll angle of the gears with and without different kinds and amounts of profile modifications.

*Keywords:* Spur gears, STE, Nonlinear, non-Hertzian
*2021 MSC:* 00-01, 99-00

## 1. Introduction

Geared transmissions are commonly used in every field of the industry to transmit, modify and repurpose mechanical shaft power and have been widely studied in literature ([1, 2]), to understand and mitigate the failures they are subjected to. In the early experimental works [3] a dynamic factor was used to compare the nominal conditions to the dynamic ones which were the cause of several types of failures. The sources of excitation of those dynamic conditions are several and very different in nature [4] and are related to the system the gears are operating in, as well as their implicit nature. Torque fluctuations are an obvious source capable of generating vibro-impacts and they are dependent on the inherent characteristics of the power source, for example an internal combustion engine [5], the unsteady aerodynamics in wind turbines [6] or drag torque in vacuum pumps [7] to cite a few examples. Also rotational

*Corresponding author: fabio.bruzzone@polito.it

speed variations, influencing sliding velocity and hence friction can cause gear vibration [8]. Backlash, manufacturing errors as well as the balancing, alignment and positioning of the shafts also play an important role ([9, 10, 11, 12]). However, the main source of excitation comes from the cyclical stiffness variation of the engaging teeth which is an inherent characteristic of gears and can be crystallized in the Static Transmission Error (STE). During the years several methods to compute that stiffness have been proposed, firstly starting from integral approaches ([13, 14]), discrete ones ([15, 16]) or considering the tooth as a trapezoidal beam on top of a rectangular one in a clamped-free condition [17]. Others proposed semi empirical formulas to describe the stiffness considering the rotational speed and the number of actual mating teeth as a function of time and contact ratio ([18, 19]). In all those approaches if contact is considered it is treated as a simple cylinder-to-cylinder contact as described in Hertzian theory [20], thus simplifying several aspects since curvature variations or edges were not considered, while also the location and load applied to the teeth are based on rigid assumptions, not considering the real conditions. With the increase of the availability and computational efficiency many researchers started using Finite Element (FE) to study firstly tooth root stresses or only the structural behavior of the tooth ([21, 22, 23]) neglecting contact entirely or considering it only as a summation of the tooth elastic effect with Hertzian phenomena up to recent years ([24, 25, 26, 27, 28]). The full extent of FE capabilities have been used only as validating tools due to their computational costs, but some hybrid approaches have been proposed, as in [29, 30] in which the FE is used to compute the elastic deflections away from the contact zone, where a detailed contact mechanics model with Semi Analytical (SA) foundations is instead introduced. In this paper a similar approach will be used to compute the STE and the influence of micro-geometrical profile modifications both on the STE and the contact pressures distributions. Indeed, a SA approach well known in literature [16] coupled with further improvements will be used to determine the stiffness of the engagement. However, the location of the contact point and the load sharing characteristics will not be assumed based on the rigid kinematics, but only employed as a starting point for a nonlinear iterative approach searching for the equilibrium of the location of the contact point, the actual number of the engaged teeth pairs and their applied load. Furthermore a detailed non-Hertzian contact mechanics model will be applied to the contacting teeth pairs in equilibrium to precisely estimate the contact pressures even in presence of profile modifications. Indeed this will allow to correctly take into account the continuous curvature variations along the flanks, as well as studying the pressure peaks when edge contact occurs. Firstly the approach to obtain the profile of the tooth is described and the semi-analytical model used to obtain the deflections under load, and hence the stiffness, is shown. Next the nonlinear iterative algorithm is described which aims at obtaining a stable global deformed configuration of the gear pair under load. At this point the non-Hertzian contact model is introduced to describe the deflections and pressure distributions in the contact zone and some results are shown to highlight the importance of a correct modeling of tip contact. Finally several results are shown for a test gear pair

are shown along with a series of comparisons of the effects of different profile modifications on the STE and the load sharing distribution and conclusions are drawn.

## 2. Model description

*Tooth geometry and contact points detection.* In order to have a general and detailed description of the gear teeth surfaces, the profiles are generated by simulating the meshing of a rack cutter tool with a gear blank by implementing the meshing interaction by vector approach as proposed by Litvin [31]. The rack cutter, shown in Figure 1, can be divided in a number of sections depending on the presence or absence of features like semi-topping, which modifies the tip surface, or the protuberance, which acts on the tooth root geometry as well as the root radius of the rack which creates a rounding on the generated tooth. In the reference frame of the cutter the main parameters defining its geometry are namely the module $m$, the pressure angle $\alpha$, the addendum coefficient $h_{\mathrm{a0}}$, the dedendum coefficient $h_{\mathrm{f0}}$, the tip radius coefficient $\rho_{\mathrm{a0}}$. Optionally, depending on the desired tooth geometry also a root radius coefficient $\rho_{\mathrm{f0}}$ can be specified, as well as the semi-topping height and angle ($h_{\mathrm{fp0}}$ and $\alpha_{\mathrm{kp0}}$ respectively) and the protuberance height and angle ($h_{\mathrm{pr,p0}}$ and $\alpha_{\mathrm{pr,p0}}$ respectively). Once the geometry is generated Tooth Profile Modification (TPM) can be further applied, such as tip relief. Other TPM as involute crowning and root relief can be applied using the proposed method, but will not be analyzed in this paper. The location of the contact points will not be defined by the intersections of the profiles with the Line Of Action (LOA) in different angular positions as done in other works ([32, 33, 34, 35]), but will be computed numerically by finding the the pair of nodes, one on the pinion and the other on the driven gear, with the minimal angular distance for each engaged tooth pair. This process will be repeated starting from the rigid conditions with the undeformed geometry as well as in every other iterative step using the deformed profiles as will be detailed later on.

*SA deflections.* The teeth profiles are discretized in $N_{\mathrm{i}}$ points and the bending and shear deformations are computed assuming the tooth as a clamped-free beam with non-uniform geometry using the analytical formula from Cornell [16] instead of the integral approach of Weber [13]. Under a tooth load $F_{\mathrm{j}}$ the expression is

$$\delta_{\mathrm{b}}^{i} = \frac{F_j \cos^2\phi_{\mathrm{l}}'}{E} \sum_{i=1}^{N_i} \delta_i \left[ \frac{l_i^2 - l_{\mathrm{i}}\delta_i + \frac{1}{3}\delta_i^2}{\bar{I}_i} + \frac{2.4(1+\nu) + \tan^2\phi_{\mathrm{l}}'}{\bar{A}_i} \right] \tag{1}$$

where $\delta_i$ is the thickness of the $i^{th}$ slice of the tooth cross-section defined by two consecutive points $i$ and $i+1$ ($i = 1, 2, ..., N_i$) of the profile. $E$ and $\nu$ are respectively the Young's modulus and Poisson coefficient of the material, while $\bar{A}_i$ and $\bar{I}_i$ are the average area and average moment of inertia of the slice, while

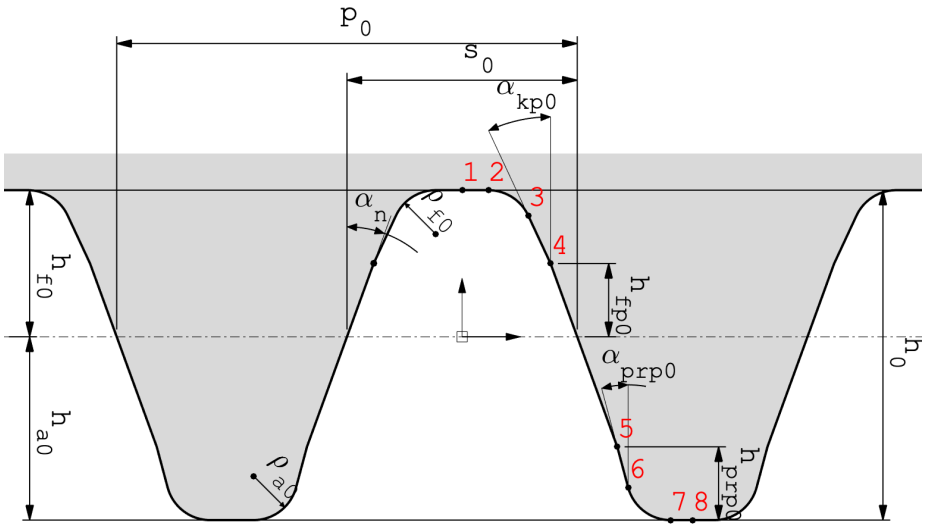


Figure 1: Rack cutter nomenclature.

$\phi'_{\rm l}$ is the working pressure angle and $l_i$ is the distance of the point of application of the load $F_j$ from the tooth base. The number of points $N_{\rm i}$ in which the tooth surface is discretized has a very low dependency on the accuracy of the obtained displacements, but a sufficient number is needed for the subsequent contact analysis to correctly represent the contact conditions, therefore in this paper each tooth will be discretized with a number of points 200 times the module $m$ in mm. The contribution to the deformation of the gear body due to the fillet and foundation compliance is based on the theory of elastic rings of Muskhelishvili [36] and its analytical expression is given as [37]

$$\delta_{\rm f}^{i} = \frac{F_j \cos^2\phi'_{\rm l}}{bE}\left[L^*\left(\frac{u}{s_{\rm f}}\right)^2 + M^*\left(\frac{u}{s_{\rm f}}\right) + P^*\left(1 + Q^*\tan^2\phi'_{\rm l}\right)\right] \tag{2}$$

where $b$ is the tooth facewidth, $u$ is the height of the intersection between the load and the tooth centerline, while $s_{\rm f}$ is the chordal thickness of the tooth root base. Coefficients $L^*$, $M^*$, $P^*$, $Q^*$ are estimated by a polynomial function of the form

$$X^*(h_{{\rm f},i}, \theta_{\rm f}) = A_i/\theta_{\rm f} + B_i h_{\rm f,i}^2 + C_i h_{{\rm f},i}\theta_{\rm f} + D_i/\theta_{\rm f} + E_i h_{{\rm f},i} + F_i \tag{3}$$

in which the parameters $h_{{\rm f},i}$ is the ratio between the root circle radius and the radius of the hub, while $\theta_{\rm f}$ is half of the tooth angular thickness. The coefficients

Table 1: Polynomial coefficients for Eq. 3

| | $A_i$ | $B_i$ | $C_i$ | $D_i$ | $E_i$ | $F_i$ |
|---|---|---|---|---|---|---|
| $L^*$ | -5.547e-5 | -1.9986e-3 | -2.3015e-4 | 4.7702e-3 | 0.0271 | 6.8045 |
| $M^*$ | 60.111e-5 | 28.100e-3 | -83.431e-4 | -9.9256e-3 | 0.1624 | 0.9086 |
| $P^*$ | -50.952e-5 | 185.50e-3 | 0.05380e-4 | 5.300e-3 | 0.2895 | 0.9236 |
| $Q^*$ | -6.2042e-5 | 9.0889e-3 | -4.0964e-4 | 7.8267e-3 | -0.1472 | 0.6904 |

$A_i$, $B_i$, $C_i$, $D_i$, $E_i$, $F_i$ are given in Table 1. By superposition, the total deflection of a tooth pair $j$ contacting at point $i$ can be defined as

$$\delta_j^i = \left(\delta_{\mathrm{b}}^i\right)_{\mathrm{p}} + \left(\delta_{\mathrm{f}}^i\right)_{\mathrm{p}} + \left(\delta_{\mathrm{b}}^i\right)_{\mathrm{g}} + \left(\delta_{\mathrm{f}}^i\right)_{\mathrm{g}} \tag{4}$$

where the subscript p indicates the deformation of the driving pinion, while g of the driven gear. Those deformations are computed for each point of the profiles and will later be applied to the 2D flanks in the procedure to obtain the equilibrium contact point. Hence, the total stiffness of the engaging teeth pair $j$ contacting in point $i$ can be expressed as

$$k_j^i = \frac{F_j}{\delta_j^i} \tag{5}$$

*Nonlinear algorithm.* It is known that a deformation during contact between two solid bodies can shift the actual contact point from its location predictable by rigid body analysis, especially if bending deformations are involved as is the case for contacting teeth pairs in gears. Indeed, if a rigid body is brought into contact via a vertical displacement with a flexible beam, the first point of contact is easily identifiable by rigid body kinematics. However, if the load is increased, the point of contact will shift, thus changing the deformed shape of the beam. The same reasoning is valid for engaging teeth pairs under load since the contact point identifiable considering the profiles as rigid (Figure 2-a) is indeed different when their deformation under load is taken into account as visible in Figure 2-b and as such cannot be determined a priori. Furthermore in gears the location of the contact point determines the stiffness which in turn determines the fraction of the total load that particular tooth pair will transmit. Numerically, this results in an iterative search in which a natural equilibrium condition is sought for the load, the position of the contact point and the deformed shape of the considered teeth pairs. To start the iterations the load is applied on the rigid contact point of the engaged pairs and the load sharing coefficient for each pair is computed using the ISO 6336 standard [38], thus obtaining the first set of deformed profiles under load. Using this deformed configuration the actual contact points are then obtained. It must be noted that in this step contact is checked between all possible pairs and both anticipated contact or contact loss can happen due to all the effects previously considered. The load sharing coefficient is then updated at the $k^{th}$ iteration using the new

contact point obtained for the $j^{th}$ pair as [39]

$$C_{k,j} = \frac{k_j}{\sum_{i=1}^{N} k_i} \left( \frac{1 + \sum_{i=1}^{N} k_i \tilde{E}_{ji}}{F} \right) \tag{6}$$

where $\tilde{E}_{ji} = \delta_j - \delta_i$ is the STE and $k_j$ is defined in eq. 5 while $F = T/r_\mathrm{b} = \sum_{j=1}^{N} F_j$ where $T$ is the total torque to be transmitted and $r_\mathrm{b}$ is the base radius of the pinion. Equilibrium is reached when the contact points of the different engaging pairs are in a stable position as well as the load sharing coefficients, meaning

$$\frac{x_{k,j} - x_{k-1,j}}{x_{k,j}} < \epsilon_\mathrm{x} \wedge \frac{y_{k,j} - y_{k-1,j}}{y_{k,j}} < \epsilon_\mathrm{y} \wedge \frac{C_{k,j} - C_{k-1,j}}{C_{k,j}} < \epsilon_C \tag{7}$$

where $x_{k,j}$, $y_{k,j}$ are the coordinates of the contact point of the $j^{th}$ engaging pair at the $k^{th}$ iteration and $\epsilon_\mathrm{x}$, $\epsilon_\mathrm{y}$ and $\epsilon_\mathrm{C}$ are tolerance values generally equal to 0.01%. Once equilibrium is reached a detailed contact model, described next, is used to study the contact between the so obtained deformed profiles. A visualization of the described iterative loop applied for every angular position is visible in Figure 3.

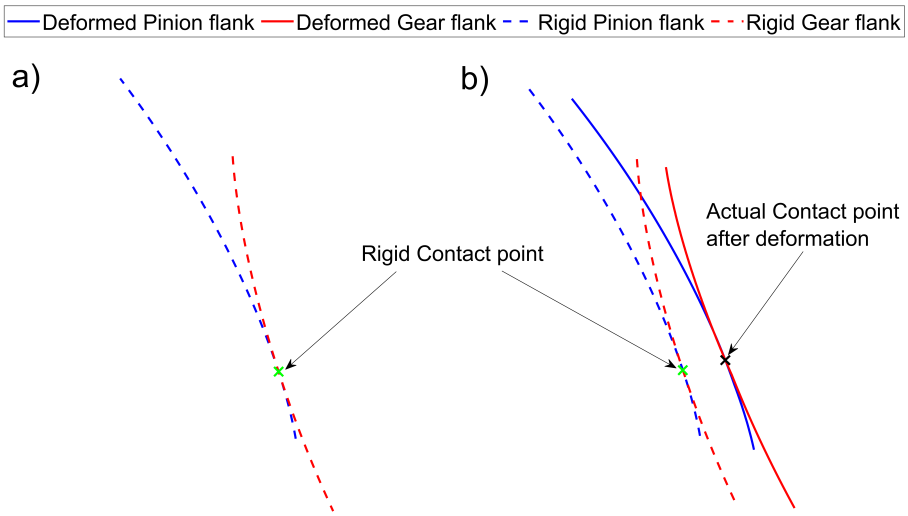


Figure 2: Shift of the actual contact point after deformation, a) rigid contact point of a single tooth pair in engagement, b) actual contact point after deformation.

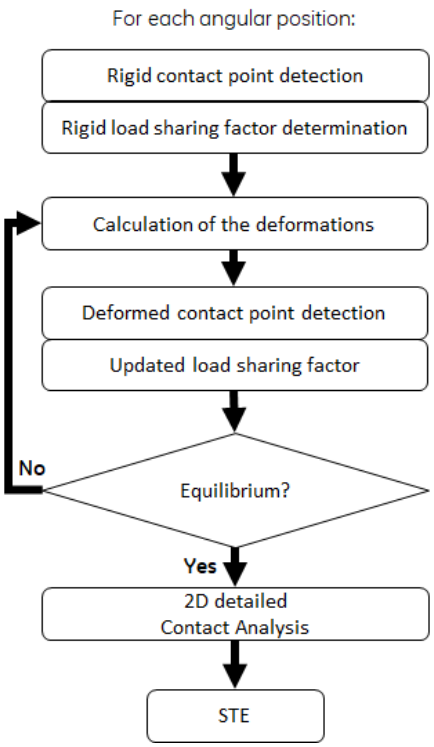


Figure 3: Pseudo-algorithm visualization.

*Non-Hertzian contact model.* Analytical or quasi-analytical contact models [40, 41] as commonly employed in literature in this kind of analytical approaches are not suitable to effectively estimate the contact stiffness and pressures distributions during engagement since they lack the capability to correctly treat the complicated geometry involved. The curvature of the teeth changes continuously due to the intrinsic nature of the involute profile and of the applied tooth deformations, and the above-mentioned models only consider the curvature at the contact point. Furthermore, when tip contact occurs there is no practical way to limit the contact area to where there actually is material to support the pressure, and similar situations occur when tooth profile modifications are to be modeled, such as linear and parabolic tip relief that will be introduced later. When high accuracy is needed the research interest is focused on the FE method [42, 43] with some exceptions [44, 45]. To overcome these limitations and obtain accurate pressure distributions and surface displacements a frictionless non-Hertzian numerical 2D line contact model was implemented. The contact conditions can be expressed in the so called Hertz-Signorini-Moreau problem [46, 47, 48]

$$\mathbf{h} \geq 0, \mathbf{p_n} \geq 0, \mathbf{h} \cdot \mathbf{p_n} = 0, \tag{8}$$

The first condition enforces that no interpenetration can occur between the contact bodies and therefore the gap function $\mathbf{h}$, which measures the distances between the surfaces, can only be positive, or equal to 0 in the contact area. The second condition imposes that the contact is non-adhesive and therefore no tension force must be present in the contact area, formulated from the normal stress

$$\boldsymbol{\sigma_n} = \mathbf{t} \cdot \mathbf{n} \tag{9}$$

where $\mathbf{t}$ is the traction force vector and $\mathbf{n}$ is the normal direction to the surface and $\mathbf{p_n} = -\boldsymbol{\sigma_n}$. The third condition enforces that the normal pressures can only be different from 0 inside the contact area where $\mathbf{h} = 0$ and null everywhere else. The gap function $\mathbf{h}$ is expressed as

$$\mathbf{h} = h_0 + \mathbf{g} + \boldsymbol{\delta} \tag{10}$$

where $h_0$ is the indentation between the profiles imposed as a rigid body motion, $\mathbf{g}$ is the initial separation of the contacting surfaces and represents it topography, while $\boldsymbol{\delta}$ represents the elastic deformation of the surfaces due to the applied normal pressure $\mathbf{p_n}$ and can be expressed as [49]

$$\boldsymbol{\delta} = \mathbf{C} \cdot \mathbf{p_n} \tag{11}$$

where $\mathbf{C}$ is a matrix of the influence coefficients which introduces the elasticity of the contacting surfaces. Its components $C_{ij}(i, j = 0, 1, \ldots N)$ relate the displacement $\delta_i$ at a point $i$ due to the application of a unit pressure at point $j$. If a pressure profile $p_{\mathrm{n}}(x)$ is assumed, the dimensionless elastic deformation

$\delta^*(x)$ can be expressed as [50]

$$\delta^*(x) = -\frac{1}{\pi}\int_{x_\mathrm{a}}^{x_\mathrm{b}} \ln|x_i - x| p_\mathrm{n}(x)\,\mathrm{d}x \tag{12}$$

If the pressure profile is approximated by a piecewise constant function $p_{\mathrm{n},j} = p_\mathrm{n}(x_j)$ in the considered region $x_j - \Delta x/2 \leq x \leq x_j + \Delta x/2$ where $\Delta x$ is the uniform mesh size $\Delta x = x_{j+1} - x_j$, then the deformation at a point $x_i = x_0 + i\Delta x$ can be written as

$$\delta^*(x_i) = -\frac{1}{\pi}\sum_{i=0}^{i=N} C^*_{ij} p_{\mathrm{n},j}\,\mathrm{d}x \tag{13}$$

where

$$C^*_{ij} = \int_{x_j-\Delta x/2}^{x_j+\Delta x/2} \ln|x_i - x|\,\mathrm{d}x \tag{14}$$

which can be solved analytically considering a constant mesh size $\Delta x = x_i - x_j = (i-j)\Delta x$ to yield

$$\begin{aligned} C_{ij} = \frac{4}{E^*}\Bigg[&\left(i-j+\frac{1}{2}\right)\Delta x \cdot \left(\ln\left|\left(i-j+\frac{1}{2}\right)\Delta x\right| - 1\right) \\ &- \left(\left(i-j-\frac{1}{2}\right)\Delta x\right)\cdot\left(\ln\left|\left(i-j-\frac{1}{2}\right)\Delta x\right| - 1\right)\Bigg] \end{aligned} \tag{15}$$

where $E^*$ is the effective elastic modulus considering the material properties of the gears in contact defined as:

$$\frac{1}{E^*} = \left(\frac{1-\nu_1^2}{E_1}\right) + \left(\frac{1-\nu_2^2}{E_2}\right) = \frac{1}{E_1^*} + \frac{1}{E_2^*} \tag{16}$$

Hence, the influence coefficients matrix $\mathbf{C}$ can be decomposed for the contacting bodies as

$$\mathbf{C} = \mathbf{C_1} + \mathbf{C_2} \tag{17}$$

where the influence coefficients of surfaces 1 and 2 are expressed by

$$\begin{aligned} C_{1,ij} = \frac{4}{E_1^*}\Bigg[&\left(i-j+\frac{1}{2}\right)\Delta x \cdot \left(\ln\left|\left(i-j+\frac{1}{2}\right)\Delta x\right| - 1\right) \\ &- \left(\left(i-j-\frac{1}{2}\right)\Delta x\right)\cdot\left(\ln\left|\left(i-j-\frac{1}{2}\right)\Delta x\right| - 1\right)\Bigg] \end{aligned} \tag{18}$$

$$\begin{aligned} C_{2,ij} = \frac{4}{E_2^*}\Bigg[&\left(i-j+\frac{1}{2}\right)\Delta x \cdot \left(\ln\left|\left(i-j+\frac{1}{2}\right)\Delta x\right| - 1\right) \\ &- \left(\left(i-j-\frac{1}{2}\right)\Delta x\right)\cdot\left(\ln\left|\left(i-j-\frac{1}{2}\right)\Delta x\right| - 1\right)\Bigg] \end{aligned} \tag{19}$$

The surfaces displacements can then be obtained from

$$\mathbf{h_s} = \mathbf{C_s p} \tag{20}$$

where $s = 1, 2$. To solve the problem stated in Eq. 8 and satisfy all the conditions a sub-iterative process is needed. Firstly, only the values $h^{\tilde{n}}$ of the nodes $\tilde{n}$ belonging to the domain $x$ that are in actual compenetration and hence satisfy

$$\tilde{n} = \{n \in x \mid h^n < 0\} \tag{21}$$

are selected to form the vector $\tilde{\mathbf{h}}$ and consistently also the corresponding rows and columns of $\mathbf{C}$ are selected to form the matrix $\tilde{\mathbf{C}}$, effectively setting all loads on nodes outside of the contact region to 0. The pressures $\tilde{\mathbf{p}}$ pertaining the compenetrating nodes are obtained by

$$\tilde{\mathbf{p}} = \tilde{\mathbf{C}}^{-\mathbf{1}}\tilde{\mathbf{h}} \tag{22}$$

Next, the list of $\tilde{n}$ nodes is updated by removing those where tensile pressures are registered and those who are not compenetrating anymore due to the elastic deflection of the contacting surfaces, leaving then only those who satisfy

$$\tilde{n} = \{n \in x \mid \mathbf{p} < 0 \wedge \mathbf{Cp} < \mathbf{h}\} \tag{23}$$

This sub-iterative process stops when the list of $\tilde{n}$ nodes at the current sub-iterative step is the same as the previous one. Finally, given a certain $h_0$ after the solution of the sub-iterative procedure just explained, the load acting on the contacting bodies for unit thickness can be found as

$$f = \frac{\Delta x}{2} \sum_{i=0}^{i=N-1} (p_{\mathrm{n},i} + p_{\mathrm{n},i+1}) \tag{24}$$

which in general will be different from the imposed load $F_{\mathrm{j}}$, hence further iterations are needed to obtain the correct $h_0$. A first guess value is used as $h_{0,1}$ for the first iteration, while for the $k^{th}$ iteration the value $h_{0,\mathrm{k}}$ to be used is estimated based on the previous iterations by

$$h_{0,k} = h_{0,k-1} + \frac{h_{0,k-1} - h_{0,k-2}}{f_k - f_{k-1}}(F_j - f_{k-1}) \tag{25}$$

with good convergence rates. The iterations stop when the residual

$$r_k = \frac{F_j - f_k}{F_j} \tag{26}$$

is below a certain tolerance value $\epsilon_{\mathrm{F}}$ so that $r_k \leq \epsilon_{\mathrm{F}}$, where usually $\epsilon_{\mathrm{F}} = 0.01\%$. A visualization of the sub-iterative algorithm to compute the pressure distribution using the proposed approach is visible in Figure 4. Since the equilibrium contact point is known through the algorithm detailed in section 2,

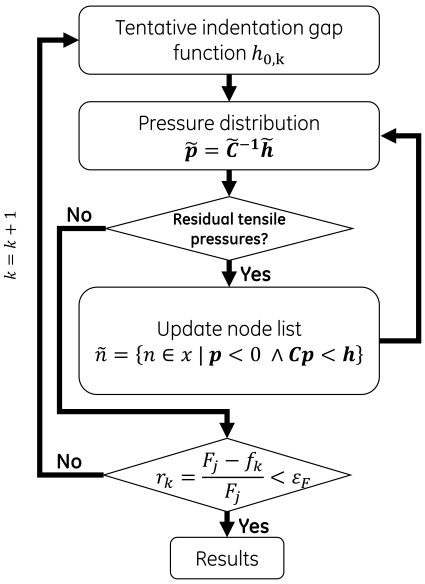


Figure 4: Visualization of the sub-iterative process to compute the pressure distribution using the non-Hertzian model.

Table 2: Gear pair parameters

| Parameter | Pinion | Gear |
|---|---|---|
| Number of teeth $z$ [-] | 28 | 28 |
| Module $m$ [mm] | 3.175 | 3.175 |
| Pressure angle $\alpha_{\mathrm{n}}$ [°] | 20 | 20 |
| Facewidth $b$ [mm] | 6.35 | 6.35 |
| Hub radius [mm] | 20 | 20 |
| Torque $T$ [Nmm] | 101686 | |
| Young modulus $E$ [MPa] | 210000 | 210000 |
| Poisson coefficient $\nu$ [-] | 0.3 | 0.3 |

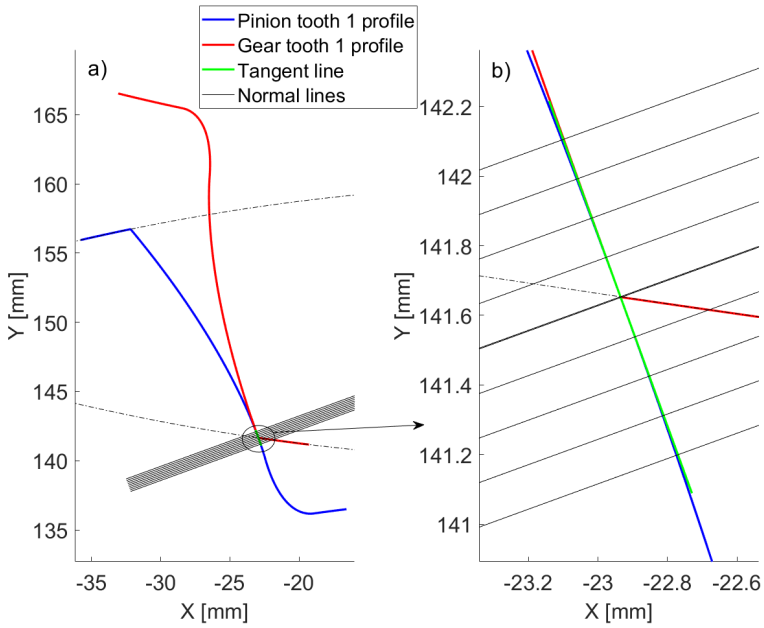


Figure 5: Initial profiles separation **g** estimation a) Full profiles, b) Zoom of the contact region.

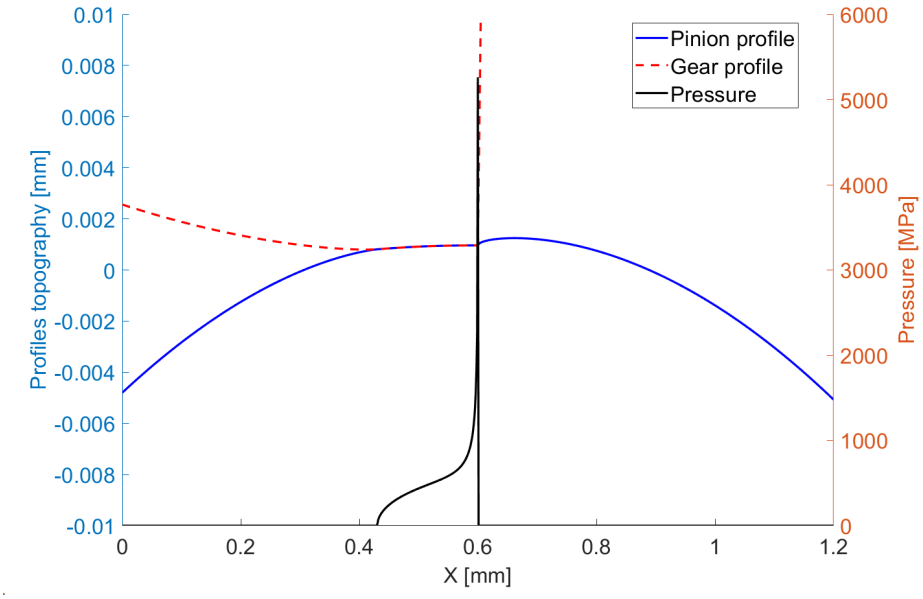


Figure 6: Gear tip contact without modifications.

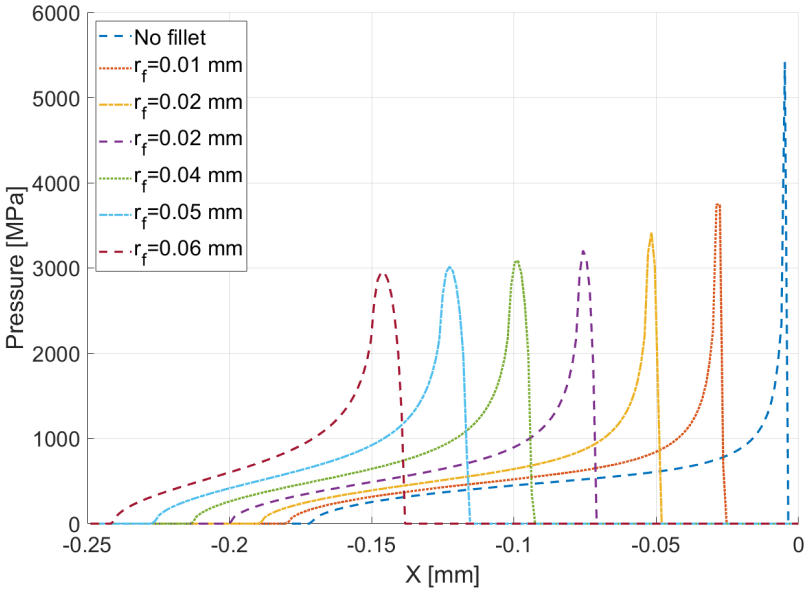


Figure 7: Effect of increasing tip fillet radius on tip contact.

the common tangent to both gear profiles is taken as the line where contact will lie. From this line the initial separation $h_0$ as the normal distance between the common tangent at the equilibrium contact point and the deformed profiles is obtained. In the cylinder–cylinder contact the imposed rigid body indentation $h_0$ was intended as a vertical displacement of either cylinder towards the other. In the pinion–gear contact instead, in order to respect the meshing kinematics, a rotation is imposed as a rigid body rotation of the pinion towards the gear. Therefore at each iteration it is needed to estimate again the initial separation $\mathbf{g_k}$ obtained through a tentative rigid body rotation $\theta_{0,k}$ for the $k^{th}$ iteration computed in the same way as Eq. 25, hence

$$\theta_{0,k} = \theta_{0,k-1} + \frac{\theta_{0,k-1} - \theta_{0,k-2}}{f_\mathrm{k} - f_{k-1}}(F_j - f_{k-1}) \tag{27}$$

The above method is valid for rough frictionless non-Hertzian contact, but it's still valid also for Hertzian problems, which allows a comparison. Two steel cylinders ($E_1 = E_2 = 210000$ MPa, $\nu_1 = \nu_2 = 0.3$) of radii $r_1 = 100$ mm and $r_2 = 20$ mm are pressed together by a load per unit length varied from 100 N to 1500 N. The maximum pressure values and the estimated contact area from the proposed method, have been compared to Hertz theory [46]. The peak pressure values and the contact area and peak pressure percentage errors are visible in Figure 8 and denote a good accuracy, with an error generally lower than 1%, and a decreasing trend as the load increases since more contact points become

part of the contact area, while in Figure 9 the deformed profiles and the pressure distribution in the contact zone are visibile for a unit length load of 1500 N.

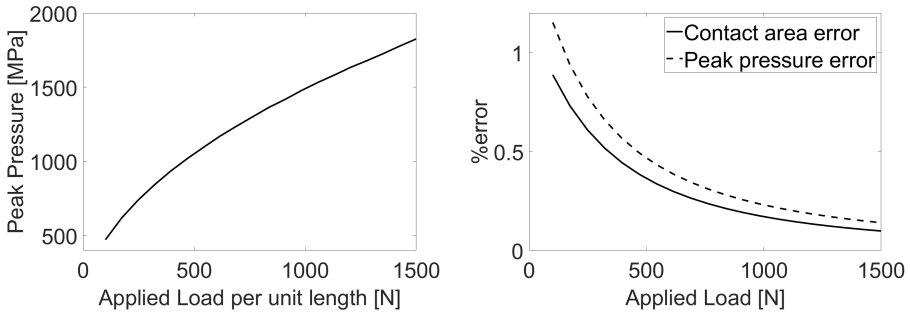


(a) Displacement distribution (b) Contact pressures

Figure 8: Peak pressure variation with increasing load (left), pressure and contact area relative percentage errors (right).

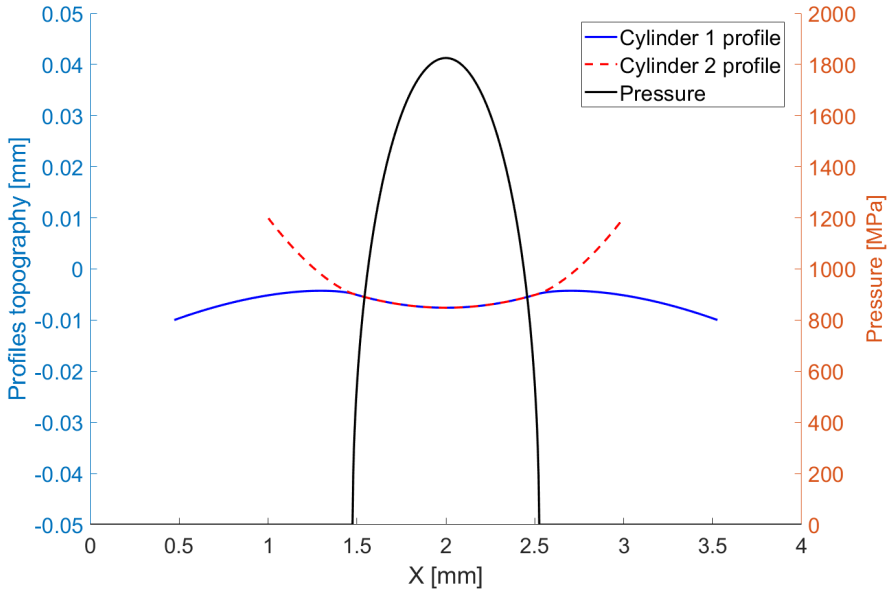


Figure 9: Deformed cylinders profiles and pressure distribution.

*Application to gear contact.* In order to test the proposed method on gear applications where the non-Hertzian approach would show results that a Hertzian approach could not correctly analyze the contact is studied in the angular position when the tip of the gear comes in contact with the flank of the pinion

as in Figure 5. The data of the gear pair considered is listed in Table 2. For a meaningful comparison only one teeth pair will be considered in contact in the position mentioned above and it will hence be applied with the full load $F = T/r_\mathrm{b}$ in order to compare the pressure distribution and highlight the influence of the different profiles modifications. The positioning of the equilibrium contact point and therefore of the contact line results from the iterative algorithm detailed in the previous paragraphs. The deformed profiles and the pressure distribution of an unmodified gear pair are shown in Figure 6 and display an important pressure peak where the sharp tip of the driven gear contacts the flank of the pinion. Although the entity of the pressure peak is exaggerated by the fact that only a single teeth pair is considered taking the full load, this is a better approach than considering the contact as Hertzian. In all upcoming graphs the 0 location of the $x$ axis will be taken as the location of the edge contact point for an unmodified gear in order to also show the different location where contact happens. Indeed, in the industry particular care is taken to avoid this kind of interaction during meshing. Even if no special measure is taken a small tip fillet radius is present due to the machining process of the gears. The magnitude of the fillet tip radius $r_\mathrm{f}$ influences the maximum value of the pressure peak and also the shape of the pressure peak as shown in Figure 7, but this reduction is limited and increasing its value even further would not decrease the overload by much. For this reason, and others as well such as minimizing the fluctuation of the STE and others, more elaborate TPM are usually introduced during manufacturing. The TPM that can be studied in a 2D case are mainly the linear and parabolic tip relief modifications.

*Influence of TPM on pressure distribution.* For the linear tip relief, the modification is characterized by the length of the material to be removed $l_\mathrm{t}$ and by the maximum amount of material to be removed at the outer diameter $\Delta_\mathrm{t}$. As the name implies the amount of material removed decreases linearly from the maximum value $\Delta_\mathrm{t}$ at the tip, to 0 after a length $l_\mathrm{t}$. Similarly, but with a parabolic trend, the parabolic tip relief is characterized by the length of the material to be removed $l_\mathrm{p}$ and by the maximum amount of material to be removed at the outer diameter $\Delta_\mathrm{p}$. Various configurations will now be analyzed to highlight the effects of those modifications on the pressure distribution when tip contact occurs, first for the linear then for the parabolic tip relief. In Figure 10 the length of the material removed $l_\mathrm{t}$ is varied from 0.1 to 0.6 mm with a constant $\Delta_\mathrm{t} = 0.02$ mm. It is evident that increasing the length reduces the maximum pressure experienced by the flank, but usually other considerations have to be taken into account since this increase would retard the approach of the profiles while anticipating the release condition thus increasing the single tooth contact region, which is not always desirable since it reduces the contact ratio. In Figure 11 the $\Delta_\mathrm{t}$ is varied from 0.05 to 0.3 mm with a constant $l_\mathrm{t} = 0.4$ mm. With those values as the material removed increases the maximum pressure increases since a sharp edge is created because a discontinuity in the curvature of the profile is created and this affects the pressure distribution. Regarding the parabolic tip relief in Figure 12 the length of the material

removed $l_p$ is varied from 0.1 to 0.6 mm with a constant $\Delta_p = 0.02$ mm. It is evident that increasing the length reduces the maximum pressure experienced by the flank up to a point where the distribution is almost Hertz-like without any asymmetric pressure peak, but again considerations on the contact ratio must be taken into account. In Figure 13 the $\Delta_p$ is varied from 0.05 to 0.3 mm with a constant $l_p = 0.4$ mm. The parabolic distribution does not cause a discontinuity in the profile of the teeth flank, but however less material is left in the contact zone and therefore a pressure peak becomes progressively more noticeable as the amount of material removed is increased. In the tip contact condition, the non-Hertzian nature of this kind of contact is extremely evident, but when the edge is not involved anymore as the meshing process continues it becomes less important. However, this approach is still more accurate since it considers the real curvature of the involute flank even considering arbitrary modifications and not just the osculating radius at the contact point with constant curvature as in classical analysis. More pressure distribution maps, with the real load distribution among the teeth in contact will be shown in the next section, and the pressure peaks as the teeth come and leave contact will still be evident in the real meshing conditions.

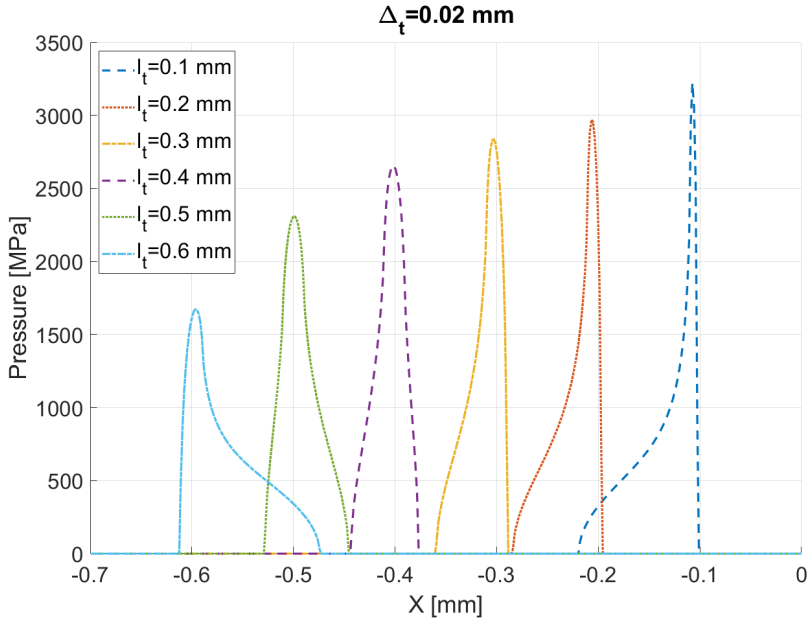


Figure 10: Effect of the increase in length $l_t$ of linear tip relief.

## 3. Application to case studies

In this section the results of the SA approach, considering the superposition of the iterative process and the detailed contact analysis, will be shown. The

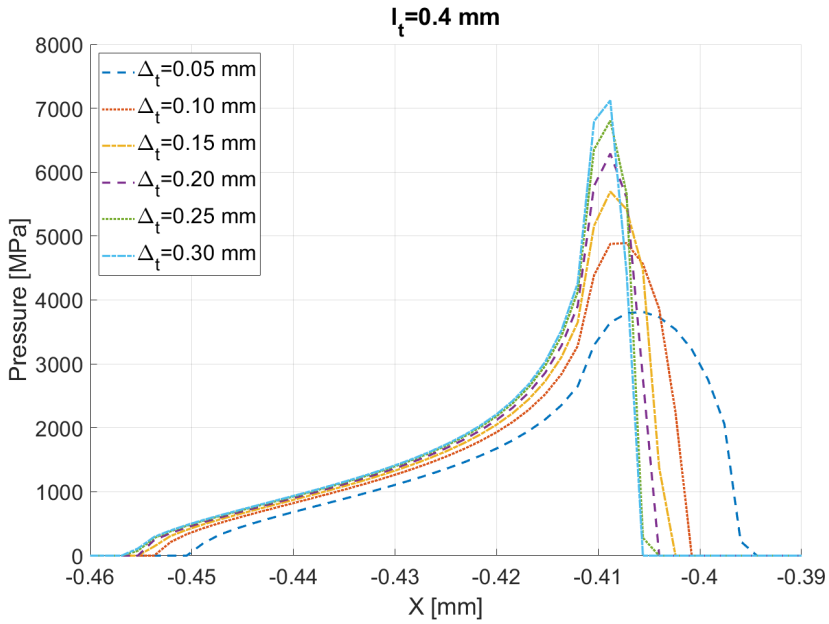


Figure 11: Effect of the increase in depth $\Delta_t$ of linear tip relief.

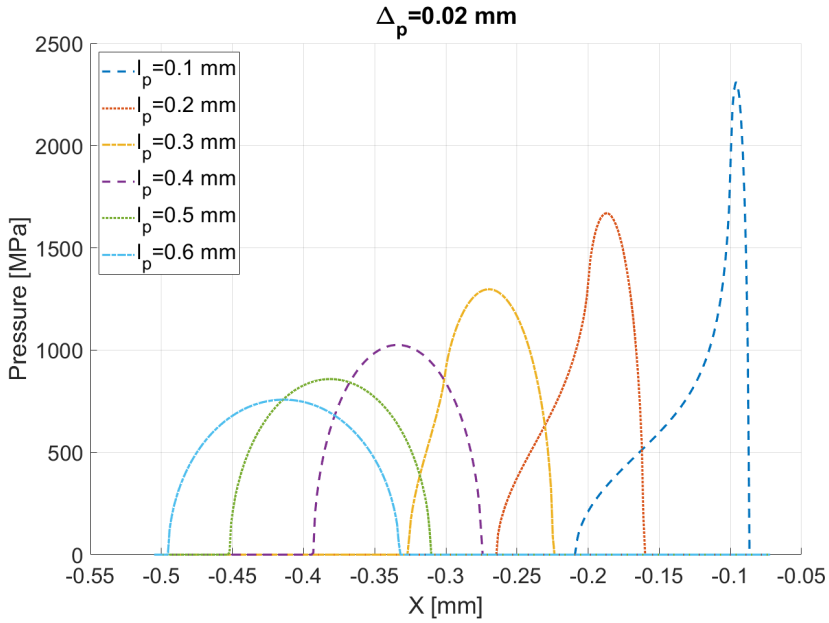


Figure 12: Effect of the increase in length $l_p$ of parabolic tip relief.

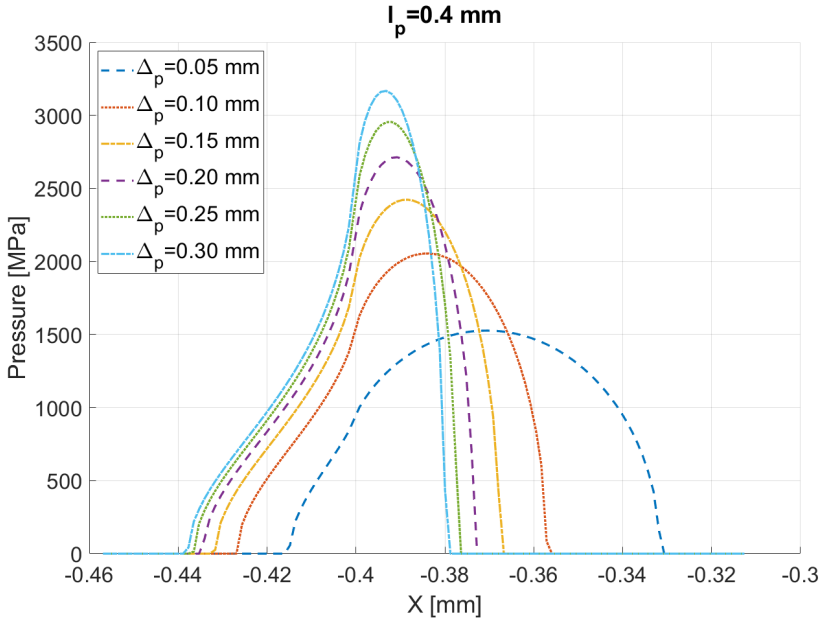


Figure 13: Effect of the increase in depth $\Delta_{\mathrm{p}}$ of parabolic tip relief.

expression for the STE is finally

$$STE = \max\left[\left(\theta_{\mathrm{g}} r_{\mathrm{b,g}} - \theta_{\mathrm{p}} r_{\mathrm{b,p}}\right)_j\right] \tag{28}$$

where the subscript p indicates the pinion rotation, while g indicates the driven gear between the j engaged teeth pairs. The rotations $\theta_{\mathrm{g}}$ and $\theta_{\mathrm{p}}$ are measured at the point of maximum displacement in the contact area from the contact analysis, therefore including also the elastic deflection $\boldsymbol{\delta_{\mathbf{p}}}$ and $\boldsymbol{\delta_{\mathbf{g}}}$. The first comparison of the results from the proposed SA model is against a 2D plane elements FE model from Ansys. In Ansys model only three teeth have been modeled in order to reduce the computational costs since a very refined mesh has been adopted for the contacting flanks of the teeth, which have a mesh size of 0.1 mm to have correct contact results, while the mesh is coarser elsewhere. Quadratic 8-node shell elements (PLANE183) have been used to discretize the geometry, while the deformable contact pair is described by pairs of frictionless contact-target elements (CONTA172-TARGE169) for 2D line contact. The geometrical and material properties are listed in Table 2. The inner diameter of the pinion gear is connected through rigid body connection RBE2 elements to a central node where the torque is applied, and the STE is recorded. The inner diameter of the driven gear is constrained in the same way, but the central node is constrained against all displacements and rotations. An example of the displacements distribution and contact pressures obtained in Ansys is visible in

Figure 14, while the obtained results for one mesh cycle and the comparison against the current method are visible in Figure 15. The agreement between the two is good in terms of overall trend, while at the single contact a difference of $0.3e^{-4}$ rad is present. Ansys results are not symmetric in the mesh cycle due to the lack of adjacent teeth and for the same reason the approach of the following tooth after single contact is slightly retarded with respect to the SA model. The second comparison that has been made has been against the results coming from the Dynamic Analysis of Spur Gear Transmissions (DANST) code from NASA [51]. The tested gears have parameters listed in Table 2 with the exceptions of the data listed in Table 3 and have been analyzed for different levels of torque ranging from 11.3 to 101.7 Nm for one mesh cycle subdivided in 85 intermediate angular positions and the results are visible in Figure 16. Again, the results compare really well except for an upward shift increasing with the torque applied which is constant throughout the meshing process and is probably caused by differences in the formulation employed to model the torsional displacement of the gear body. The two models agree particularly well in the determination of the reduction of the single contact portion of the engagement. In both comparisons no TPM was applied to the gears, but the effect to various levels of torque, ranging from 25.4 Nm to 305.1 Nm, for the same gears tested on the NASA code but this time with a linear tip relief ($\Delta_t = 0.0032$ mm, $l_t = 0.96$ mm) symmetric on both gears are analyzed in Figure 17 over two mesh cycles. As the torque increases also the mean value of the STE increases, but the region of single tooth contact strongly reduces, closely approaching the value of 2 for the highest level of torque. As further comparison the computed gearmesh stiffness obtained from a similar analytical model by Chaari *et al.* [33] is compared to the results from the proposed SA model in Figure 18. Since both models are based on essentially the same formulation the gearmesh stiffness values in single and double contact are extremely close to each other. However small differences can be appreciated since in the proposed SA approach the contact point locations are not based on the geometrical intersections of the profiles with the LOA, thus slightly altering the stiffness values. Furthermore the single contact region is smaller in the proposed approach due to the effect of tooth flexibility under load in the iterative search of the contacting pairs, which is neglected in [33], while also the trend is asymmetric in the mesh cycle since the studied gears have different number of teeth. In the present example the differences are small since the applied torque is low in respect to the stiffness of the studied gear pair, but with higher torque or increased tooth flexibility the differences would be even more evident. In Figure 19 a single STE for the geometry earlier analyzed in the Ansys and DANST comparisons under a torque of 101.7 Nm is visible alongside with the load sharing coefficients for the different engaging teeth pairs.The pressure distribution along the entire mesh process in these conditions is visible Figure 20 and displays the pressure peak as expected and discussed in the previous paragraph. The maximum pressure value is a lot lower than what visible in Figure 6 since in the present case the load acting at the beginning of contact is lower. However, this condition could still cause damage to the flank since the maximum pressure value at the beginning of contact is

Table 3: Gear pair parameters -DANST comparison

| Parameter | Pinion | Gear |
|---|---|---|
| Hub radius [mm] | 10 | 10 |
| Young modulus $E$ [MPa] | 206800 | 206800 |
| Poisson coefficient $\nu$ [-] | 0.29 | 0.29 |

equal to 1414 MPa, which is larger than the maximum value in the single contact zone of the mesh cycle which is 992 MPa, and is usually the value for which gears are designed for. If not accounted for, this pressure peak could cause for example pitting on its surface and must hence be avoided.

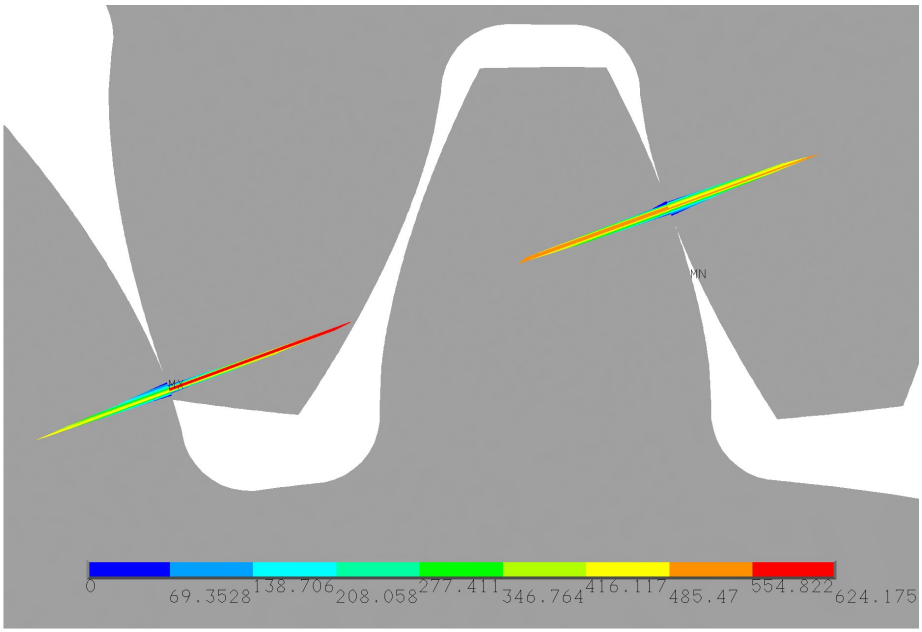


Figure 14: Contact pressures obtained from Ansys at position 0.1/1 in the mesh cycle.

The effect of the linear tip relief is now analyzed. In Figure 21 the effect of the amount of material removed $\Delta_t$ is visible for a fixed length of $l_t = 0.96$ mm. The values are varied from a minimum of 0.01 mm up to 0.04 mm. The main effect is that, as the material removed increases, the length of the single contact zone increases since the teeth pair engage later and leave contact sooner than normal, effectively decreasing the expected contact ratio and leaving the peak to peak value of the STE unchanged. Also, the load sharing coefficient doesn't improve since the passage from double to single contact becomes even more abrupt as the material removed increases, while in the double contact zone the values remain unchanged. In Figure 22 the effect of the length of the linear tip relief is analyzed alongside with the changes it creates in the load

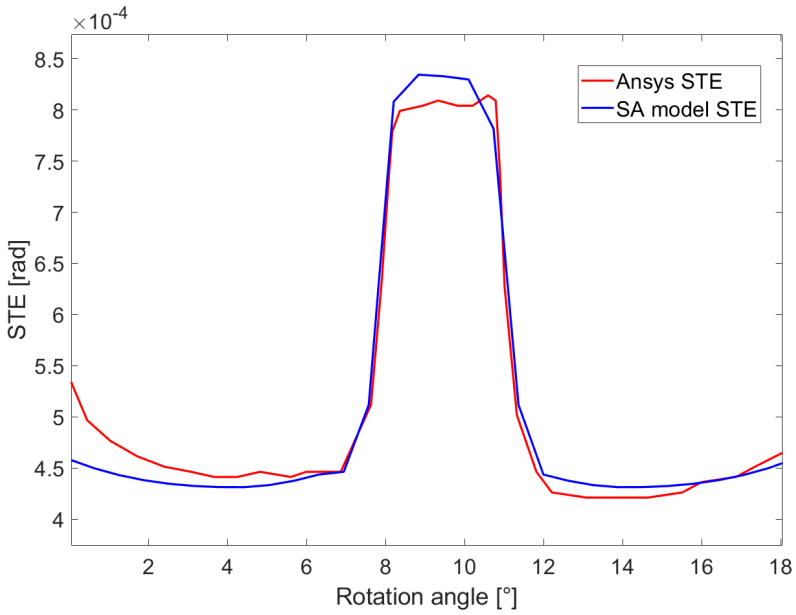


Figure 15: STE results from Ansys and Semi Analytical model.

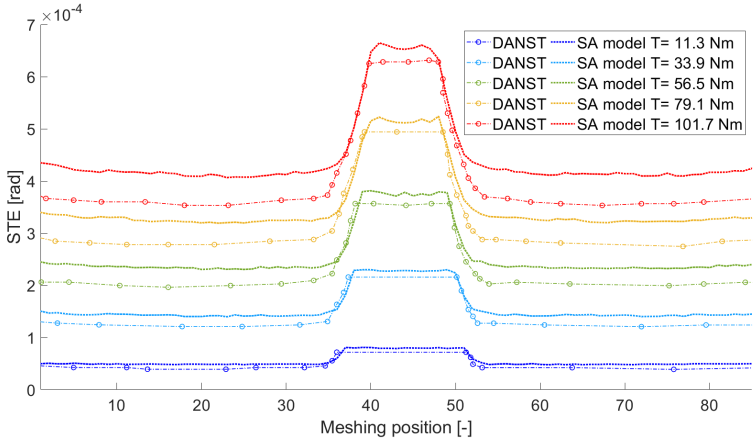


Figure 16: Comparison of NASA DANST results and SA model for several torques.

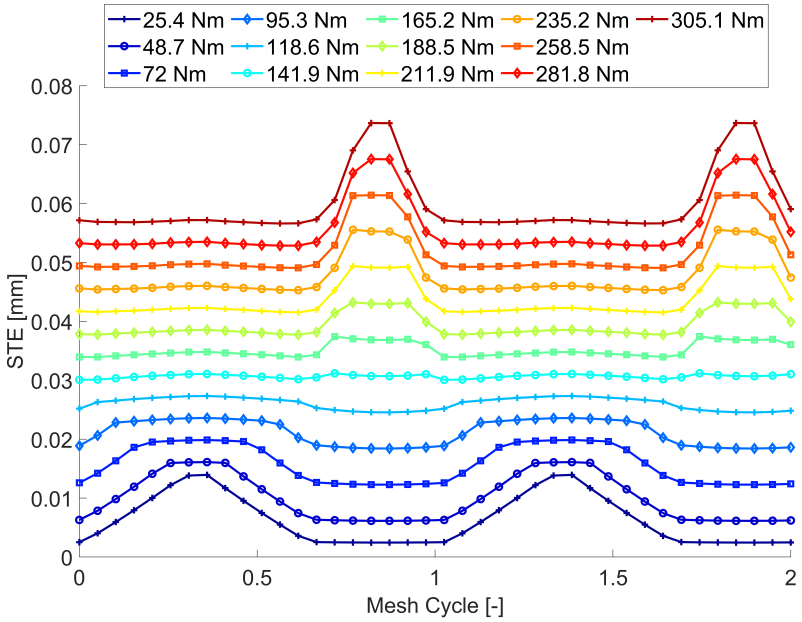


Figure 17: Effect of torque on gears with linear tip relief.

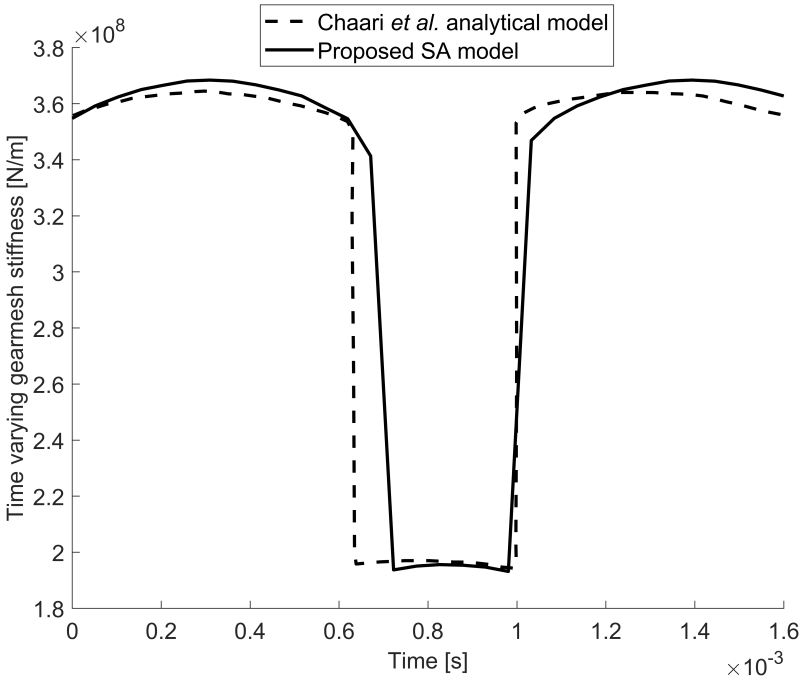


Figure 18: Comparison of gearmesh stiffness from [33] and the proposed SA model.

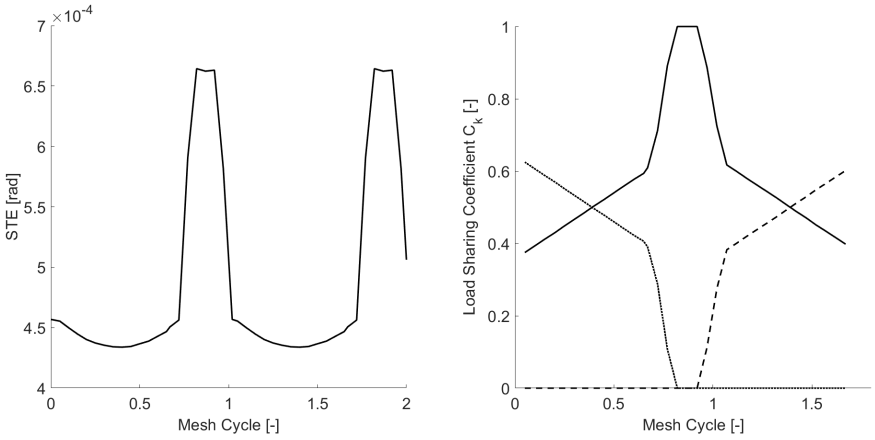


Figure 19: STE and load sharing coefficients without TPM.

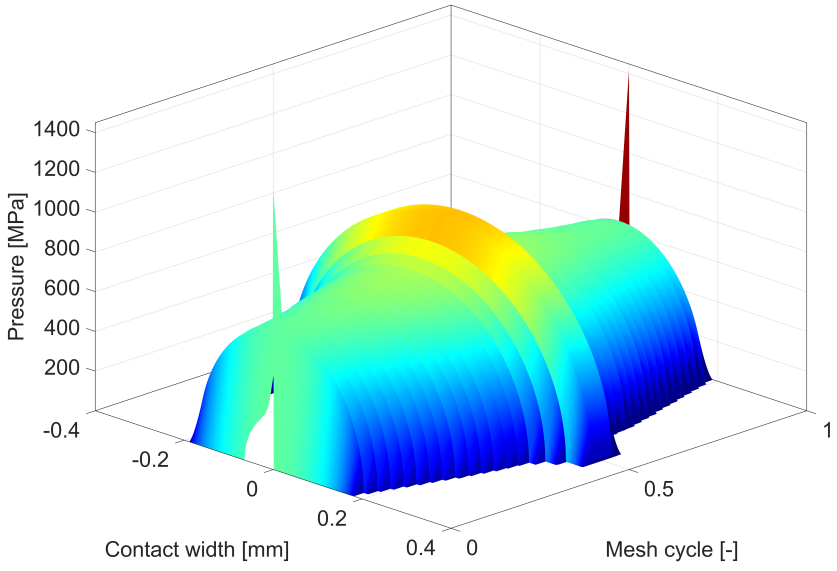


Figure 20: Pressure distribution along the entire mesh process without TPM.

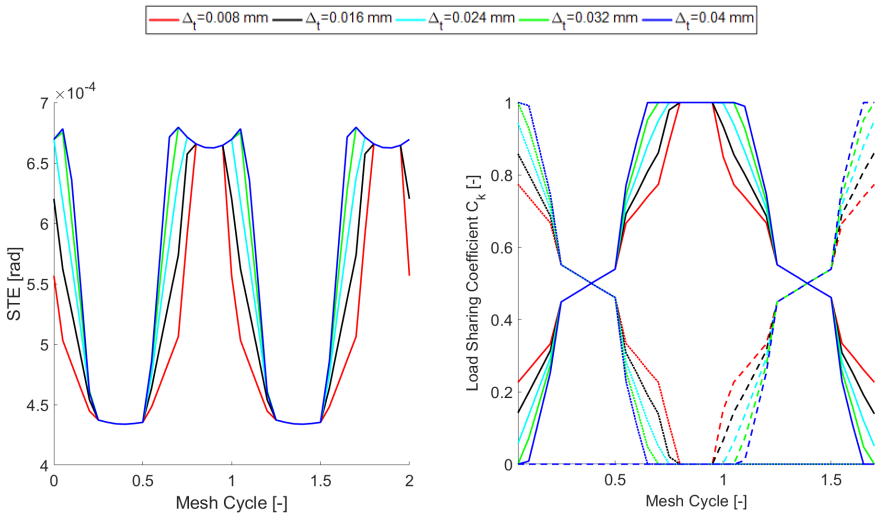


Figure 21: Effect of the variation of the amount of the material removed $\Delta_t$ in linear tip relief TPM $l_t = 0.96$ mm.

sharing coefficients. The length of the material removed $l_t$ is varied from 0.96 mm up to 3 mm and in this case some improvements on both the STE and the load sharing coefficients can be appreciated. Indeed, after a certain value the minimum value of the STE can be seen to increase thus effectively reducing its peak to peak value and at the same time smoothing the transition between the teeth since the fraction of the total load they experience changes without evident discontinuities. In Figure 23 the contact pressure on the flank during the mesh process can be observed for a linear tip relief TPM with $l_t = 0.96$ mm and $\Delta_t = 0.032$ mm and it can be seen that thanks to this modification the pressure peak as the tooth comes into contact is reduced with respect to the unmodified case as in Figure 20. The peak value is equal to 1031 MPa which is still higher than the maximum pressure in the single contact zone of the mesh cycle but is less dangerous than the previous case, since it's only around 40 MPa higher than the design value.

In Figure 24 the effect on the STE and the load sharing coefficients of the amount of material removed in a parabolic tip relief is visible. Its effects are similar to those of the linear tip relief since its only effect is to increase the fraction of the mesh cycle during which single contact occurs. The peak to peak value of the STE remains constant and the load sharing variation doesn't show evident beneficial effects. In Figure 25 the effect of the length of the parabolic tip relief is analyzed and in this case, similarly to what happens for the linear tip relief, some improvements can be seen. As the length of the material removed increase the minimum value of the STE increases and therefore the peak to peak ratio decreases. At the same time, the variation of the load sharing coefficients become smoother as the variation becomes more gradual.

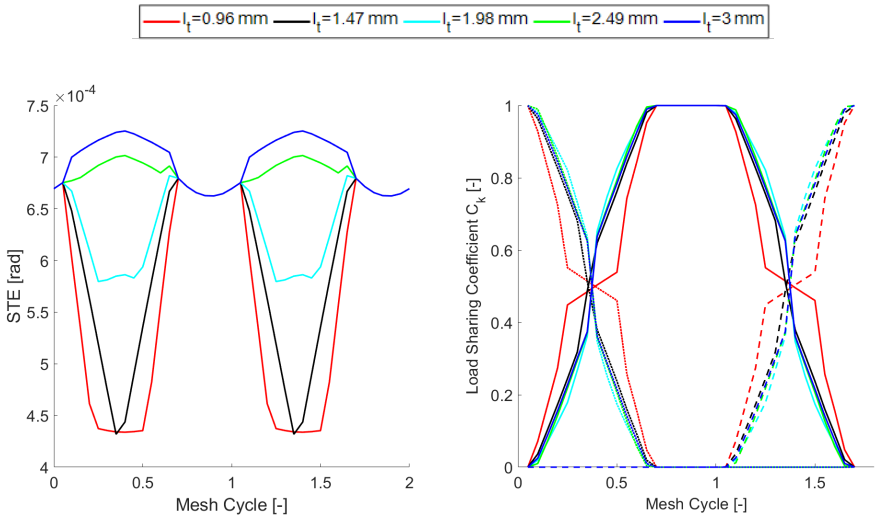


Figure 22: Effect of the variation of the length of the material removed $l_{\mathrm{t}}$ in linear tip relief TPM $\Delta_{\mathrm{t}} = 0.032$ mm.

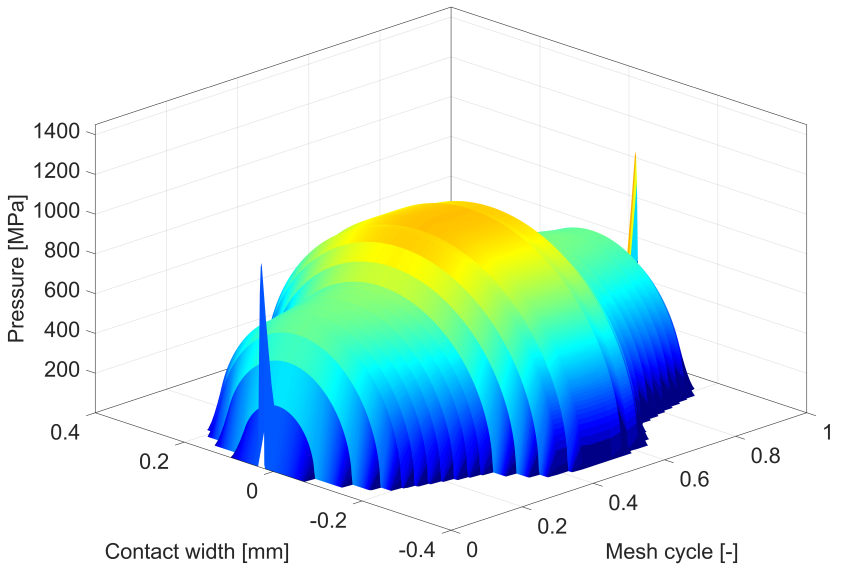


Figure 23: Pressure distribution along the entire mesh process with linear tip relief $l_{\mathrm{t}} = 0.96$ mm and $\Delta_{\mathrm{t}} = 0.032$ mm.

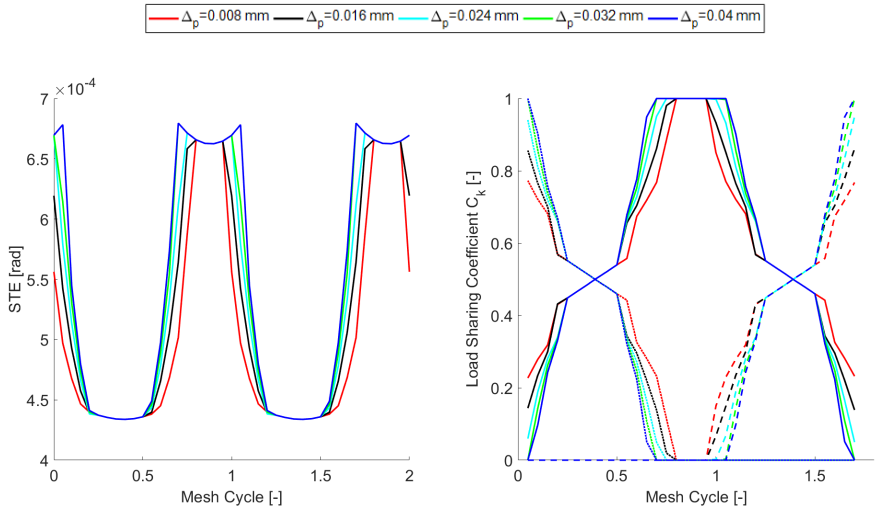


Figure 24: Effect of the variation of the length of the material removed $\Delta_{\mathrm{p}}$ in parabolic tip relief TPM $l_{\mathrm{p}} = 0.96$ mm.

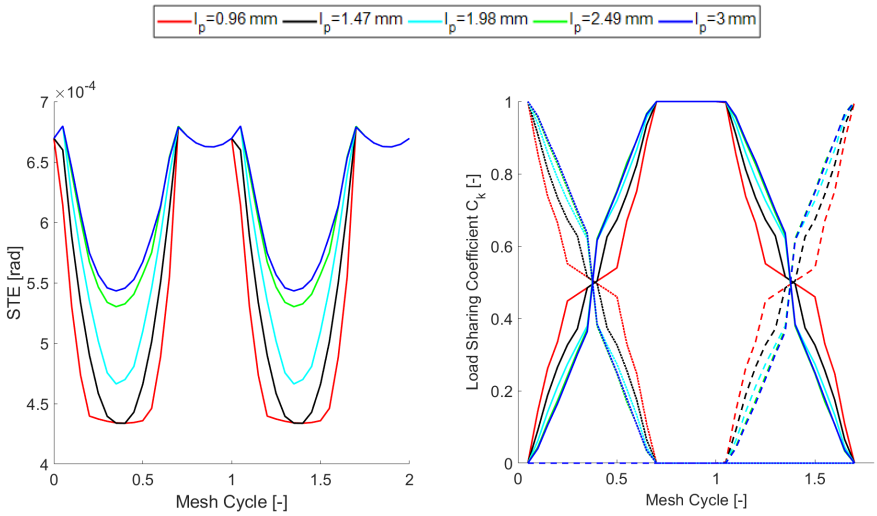


Figure 25: Effect of the variation of the length of the material removed $l_{\mathrm{p}}$ in parabolic tip relief TPM $\Delta_{\mathrm{p}} = 0.032$ mm.

The effect of this modification is lower with respect to the linear tip relief and indeed for the same values of modification the reduction in the peak to peak value of the STE is lower. This is due to the different geometry of the two kind of modifications, since for the same values the volume effectively removed is higher for the linear tip relief, since the amount of material removed increases faster than with respect to the parabolic one. However, the pressure distribution along the entire mesh process for a gear modified with parabolic tip relief with $l_\mathrm{p} = 0.96$ mm and $\Delta_\mathrm{p} = 0.032$ mm can be seen in Figure 26 and this kind of modification is evidently more effective in reducing the pressure peak as the flanks of the gears come into contact. Indeed, the peak is almost completely eliminated (481 MPa) and is just slightly higher than the pressure value when the tip contact effect disappears (430 MPa), but still less than half of the design value in the single tooth contact portion of the mesh cycle and therefore poses no dangers to the integrity of the flank surface.

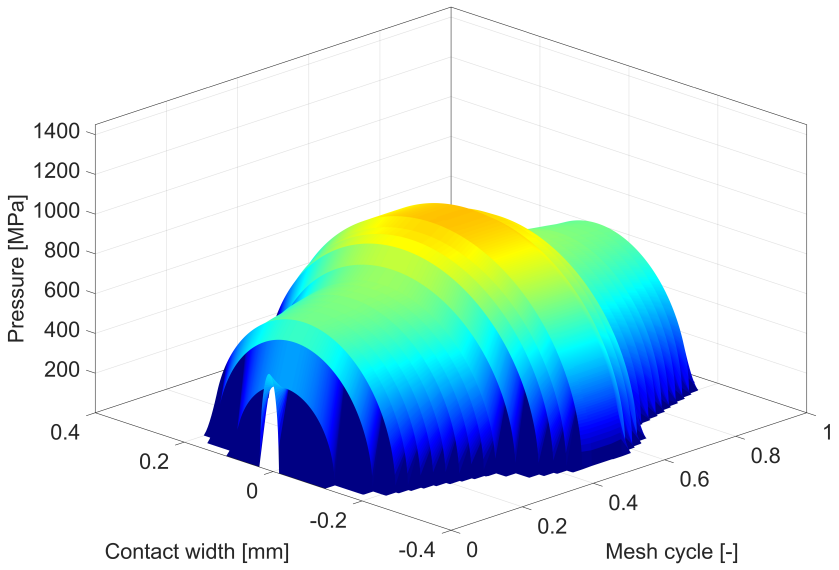


Figure 26: Pressure distribution along the entire mesh process with parabolic tip relief $l_\mathrm{p} = 0.96$ mm and $\Delta_\mathrm{p} = 0.032$ mm.

## 4. Conclusions

Even though gears have been deeply studied and have widespread applications this research field is ever growing. In this paper a novel approach to determine the STE has been detailed. Based on SA foundations well established

in literature regarding the generation of the tooth and the basic stiffness and deformation, this model introduces novel features. A nonlinear iterative approach has been implemented to determine the number of actual engaged tooth pairs, the location of the contact point and the load sharing characteristics without a priori assumptions regarding the position along the line of action or the mesh cycle. This has been achieved aiming for an equilibrium condition of the SA model in terms of deformations and load. Furthermore, whereas in literature the contact between gears is commonly treated with simplified approaches, like considering it as a cylinder-cylinder contact with constant curvature radii, here it has been treated in much more detail. A non-Hertzian contact mechanics model has been applied to the equilibrium deformed profiles to study particular conditions, usually neglected, such as the tip contact that can happen when a teeth pair begins its engagement. Several results have been presented to expose the effects that different TPM can have on this phenomenon. After a validation of the accuracy of the approach against a FE model and results available in literature finally results of the complete approach in terms of STE, load sharing characteristics and contact pressures along the engagement have been shown for different combinations of TPM and their differences and effects have been highlighted. The results given here are just examples of the capabilities of the proposed model, but it is clear that in order to achieve a good gear design those analyses alone are not enough. Indeed, a combinatory analysis taking into account the design loads and the possible combination of the macro (module, pressure angle, profile shift, etc.. . . ) and micro (tip or root relief, kind of TPM, length and amount of material removed) have to be considered at the same time so as to create a response surface in which the effects of all parameters are linked and can therefore be used to estimate the better combination to improve the reliability, wear resistance, fatigue life or noise related issues depending on the objective or objectives of the analysis. This optimization approach, common in literature ([52, 53, 54]), is not in the scope of the current work but will be object of future research.

**List of Abbreviations**

**DANST** Dynamic Analysis of Spur Gear Transmissions. 19

**FE** Finite Element. 2

**LOA** Line Of Action. 3

**SA** Semi Analytical. 2

**STE** Static Transmission Error. 2

**TPM** Tooth Profile Modification. 3

## References


[1] B. Abersek, J. Flasker, S. Glodez, Review of mathematical and experimental models for determination of service life of gears, Engineering Fracture Mechanics 71 (2004) 439–453.

[2] L. Prasil, J. Mackerle, Finite element analyses and simulations of gears and gear drives, a bibliography 1997-2006, International Journal for Computer-Aided Engineering and Software 25 (2008) 196–219.

[3] H. N. Ozguven, D. R. Houser, Mathematical models used in gear dynamics - a review, Journal of Sound and Vibration 121 (1988) 383–411.

[4] F. Bruzzone, C. Rosso, Sources of excitation and models for cylindrical gear dynamics: a review, Machines 8 (2020) 37.

[5] Y. Kadmiri, J. Perret-Liaudet, E. Rigaud, A. Le Bot, L. Vary, Influence of multiharmonics excitation on rattle noise in automotive gearboxes, Advances in Acoustics and Vibration 2011 (2011) 659797.

[6] I. Bel Mabrouk, A. El Hami, L. Walha, B. Zghal, Dynamic vibrations in wind energy systems: Application to vertical axis wind turbine, Mechanical Systems and Signal Processing 85 (2017) 396–414.

[7] P. Garambois, G. Donnard, E. Rigaud, J. Perret-Liaudet, Multiphysics coupling between periodic gear mesh excitation and input/output fluctuating torques: Application to a roots vacuum pump, Journal of Sound and Vibration 405 (2017) 158–174.

[8] H. Jiang, F. Liu, Dynamic modeling and analysis of spur gears considering friction–vibration interactions, Journal of Brazilian Society of Mechanical Science and Engineering 39 (2017) 4911–4920.

[9] S. Theodossiades, S. Natsiavas, Non-linear dynamics of gear-pair systems with periodic stiffness and backlash, Journal of Sound and Vibration 229 (2000) 287–310.

[10] J. Hedlund, A. Lehtovaara, Testing method for the evaluation of parametric excitation of cylindrical gears, Nondestructive Testing and Evaluation 23 (2008) 285–299.

[11] N. Inavolu, S. N. Kamani, R. M. Jaganmohan, Driveline noise source identification and reduction in commercial vehicles, SAE Technical Paper 2018-01-1474.

[12] F. Guo, Z. Fang, The statistical analysis of the dynamic performance of a gear system considering random manufacturing errors under different levels of machining precision, Proceedings of the Institution of Mechanical Engineers, Part C: Journal of Mechanical Engineering Science 234 (2020) 3–18.

[13] C. Weber, The deformation of load gears and the effect on their load-carrying capacity. Technical Report no. 3, British Department of Scientific and Industrial Research, London, 1949.

[14] C. Weber, K. Banaschek, Formänderung und Profilrücknahme be gerad- und schraegverzahnten Raedern, Vieweg, Braunschweig, 1953.

[15] R. W. Cornell, W. W. Westervelt, Dynamic tooth loads and stressing for high contact ratio spur gears, Transactions of the American Society of Mechanical Engineers, Journal of Mechanical Design 100 (1978) 69–76.

[16] R. W. Cornell, Compliance and stress sensitivity of spur gear teeth, Journal of Mechanical Design 103 (1981) 447–459.

[17] J. Ishikawa, Fundamental investigations on the design of spur gears, Bull of T.I.T 197 (1957) 55–62.

[18] Y. Cai, T. Hayashi, The optimum modification of tooth profile of power transmission spur gears to make the rotational vibration equal zero, Transactions of the Japan Society of Mechanical Engineers 57 (1991) 3957–3963.

[19] Y. Cai, T. Hayashi, The linear approximated equation of vibration of a pair of spur gears, Journal of Mechanical Design 116 (1994) 558–564.

[20] H. R. Hertz, Über die berührung fester elastischer Körper, Zeitschrift für die reine und angewandte Mathematik 92 (1881) 156–171.

[21] G. Deng, T. Nakanishi, K. Inoue, Bending load capacity enhancement using an asymmetric tooth profile, JSME International Journal Series C 46 (2003) 1171–1177.

[22] T. Lin, H. Ou, R. Li, A finite element method for 3d static and dynamic contact/impact analysis of gear drives, Computer Methods in Applied Mechanics and Engineering 196 (2007) 1716–1728.

[23] N. L. Pedersen, M. F. Jorgenses, On gear tooth stiffness evaluation, Computers and Structures 135 (2014) 109–117.

[24] M. H. Arafa, M. M. Megahed, Evaluation of spur gear mesh compliance using the finite element method, Proceedings of the Institution of Mechanical Engineers, Part C: Journal of Mechanical Engineering Science 213 (1999) 569–579.

[25] W. Hu, Z. Chen, A multi-mesh mpm for simulating the meshing process of spur gears, Computers and Structures 81 (2003) 1991–2002.

[26] J. D. Wang, I. M. Howard, Error analysis of finite element modeling of involute spur gears, Journal of Mechanical Design 128 (2006) 90–97.

[27] S. He, R. Gunda, R. Singh, Effect of sliding friction on the dynamics of spur gear pair with realistic time-varying stiffness, Journal of Sound and Vibration 301 (2007) 927–949.

[28] S. Li, Finite element analyses for contact strength and bending strength of a pair of spur gears with machining errors, assembly errors and tooth modifications, Mechanism and Machine Theory 42 (2007) 88–114.

[29] R. G. Parker, S. M. Vijayakar, T. Imajo, Non-linear dynamic response of a spur gear pair: Modelling and experimental comparisons, Journal of Sound and Vibration 237 (2000) 435–455.

[30] Y. Guo, T. Eritnel, T. M. Ericson, R. G. Parker, Vibro-acoustic propagation of gear dynamics in a gear-bearing-housing system, Journal of Sound and Vibration 333 (2014) 5762–5785.

[31] F. L. Litvin, Gear geometry and applied theory, P. T. R. Prentice Hall, 1994.

[32] A. Fernandez del Rincon, F. Viadero, M. Iglesias, A. de Juan, R. Sancibrian, A model for the study of meshing stiffness in spur gear transmissions, Nondestructive Testing and Evaluation 61 (2013) 30–58.

[33] F. Chaari, T. Fakhfakh, M. Haddar, Analytical modelling of spur gear tooth crack and influence on gearmesh stiffness, European Journal of Mechanics - A/Solids 28 (2009) 461–468.

[34] A. Y. Tesfahuneng, F. Rosa, C. Gorca, The effects of the shape of tooth profile modifications on the transmission error, bending and contact stress of spur gears, Proceedings of the Institution of Mechanical Engineering Part C: Journal of Mechanical Engineering Science 224 (2010) 1749–1758.

[35] V. Nikolic, C. Dolicanin, D. Dimitrijevic, Dynamic model for the stress and strain state analysis of a spur gear transmission, Journal of Mechanical Engineering 58 (2012) 56–67.

[36] N. Muskhelishvili, Some basic problems of the mathematical theory of elasticity, Springer Netherlands, Heidelberg, 1975.

[37] P. Sainsot, P. Velex, O. Duverger, Contribution of gear body to tooth deflections - a new bidimensional analytical formula, Journal of Mechanical Design 126 (2004) 748–752.

[38] ISO 6336-1:2019 Calculation of load capacity of spur and helical gears, Standard, International Organization for Standardization, Geneva, CH (2019).

[39] H. Ma, X. Pang, R. J. Feng, J. Zeng, B. C. Wen, Improved time-varying mesh stiffness model of cracked spur gears, Engineering Failure Analysis 55 (2015) 271–287.

[40] P. Sainsot, P. Velex, On contact deflection and stiffness in spur and helical gears, Mechanism and Machine Theory 154 (2020) 104049.

[41] V. I. Medvedev, A. E. Volkov, M. A. Volosova, O. E. Zubelevich, Mathematical model and algorithm for contact stress analysis of gears with multi-pair contact, Mechanism and Machine Theory 86 (2015) 156–171.

[42] H. X., Z. Fang, X. Zhang, Static contact analysis of spiral bevel gear based on modified VFIFE (vector form intrinsic finite element) method, Applied Mathematical Modelling 60 (2018) 192–207.

[43] A. Beinstingel, M. Keller, M. Heider, B. Pinnekamp, S. Marburg, A hybrid analytical-numerical method based on isogeometric analysis for determination of time varying mesh stiffness, Mechanism and Machine Theory 154 (2020) 104049.

[44] N. Pop, S. Cretu, A. Tufescu, Non-hertzian contact model for tooth contact analysis of spur gear with lead crowning, Applied Mechanics and Materials 658 (2014) 351–356.

[45] Q. Wen, Q. Du, X. Zhai, An analytical method for calculating the tooth surface contact stress of spur gears with tip relief, International Journal of Mechanical Sciences 151 (2019) 170–180.

[46] K. L. Johnson, Contact mechanics, Cambridge University Press, Cambridge, 1985.

[47] J. J. Kalker, Three-dimensional elastic bodies in rolling contact, Springer Netherlands, 1990.

[48] P. Wriggers, Computational contact mechanics, Springer, 2002.

[49] R. S. Sayles, Basic principles of rough surface contact analysis using numerical methods, Tribology International 29 (1996) 639–650.

[50] C. H. Venner, Multilevel solution of the EHL line and point contact problems, Ph.D Thesis, University of Twente, Twente, 1963.

[51] F. B. Oswald, H. H. Lin, R. Delgado I., Dynamic analysis of spur gear transmissions (DANST). pc version 3.00 user manual, NASA Technical Report 107291 (1996) 1–26.

[52] N. Amini, B. G. Rosen, H. Westberg, Optimization of gear tooth surfaces, International Journal of Machine Tools and Manufacture 38 (1998) 425–435.

[53] A. L. Kapelevich, Y. V. Shekhtman, Direct gear design: Bending stress minimization, Gear Technology 20 (2003) 44–47.

[54] Y. M. Mohan, T. Seshaiah, Spur gear optimization by using genetic algorithm, International Journal of Engineering Research and Applications 2 (2012) 331–318.